

# Wasserstein Gradient Boosting: A Framework for Distribution-Valued Supervised Learning

Takuo Matsubara  
The University of Edinburgh  
takuo.matsubara@ed.ac.uk

## Abstract

Gradient boosting is a sequential ensemble method that fits a new weaker learner to pseudo residuals at each iteration. We propose Wasserstein gradient boosting, a novel extension of gradient boosting that fits a new weak learner to alternative pseudo residuals that are Wasserstein gradients of loss functionals of probability distributions assigned at each input. It solves distribution-valued supervised learning, where the output values of the training dataset are probability distributions for each input. In classification and regression, a model typically returns, for each input, a point estimate of a parameter of a noise distribution specified for a response variable, such as the class probability parameter of a categorical distribution specified for a response label. A main application of Wasserstein gradient boosting in this paper is tree-based evidential learning, which returns a distributional estimate of the response parameter for each input. We empirically demonstrate the superior performance of the probabilistic prediction by Wasserstein gradient boosting in comparison with existing uncertainty quantification methods.

## 1 Introduction

Gradient boosting is a celebrated machine learning algorithm that has achieved considerable success with tabular data [1]. Gradient boosting has been extensively used for point forecasts and probabilistic classification, yet a relatively small number of studies have been concerned with the predictive uncertainty of gradient boosting. Predictive uncertainty of machine learning models plays a growing role in today’s real-world production systems [2]. It is vital for safety-critical systems, such as medical diagnoses [3] and autonomous driving [4], to assess the potential risk of their actions that partially or entirely rely on predictions from their models. Gradient boosting has already been applied in a diverse range of real-world applications, including click prediction [5], ranking systems [6], scientific discovery [7], and data competition [8]. There is a pressing need for methodology to harness the power of gradient boosting to predictive uncertainty quantification.

In classification and regression, we typically specify a noise distribution  $p(y | \theta)$  of a response variable  $y$  and use a model to return a point estimate  $\theta(x)$  of the response parameter for each input  $x$ . In recent years, the importance of capturing uncertainty in the model output  $\theta(x)$  has increasingly been emphasised [2]. A variety of approaches have been proposed to obtain a distributional estimate  $p(\theta | x)$  of the response parameter for each input  $x$  [e.g. 9, 10, 11]. For example, Bayesian neural networks (BNNs) quantify uncertainty in network weights and propagate it to the space of network outputs. Marginalising the predictive distribution  $p(y | \theta)$  over the distributional estimate  $p(\theta | x)$  has been demonstrated to confer enhanced predictive accuracy and robustness against adversarial attacks [11]. Furthermore, the dispersion of the distributional estimate has been used as a powerful indicator for out-of-distribution (OOD) detection [12].

In this context, a line of research based on the concept of *evidential learning* has recently gained significant attention [11, 13, 14, 15]. The idea can be interpreted as making use of the ‘individual-level’ posterior  $p(\theta | y_i)$  of the response parameter  $\theta$  conditional on each individual datum  $y_i$ , which arises from the response-distribution likelihood  $p(y_i | \theta)$  and a user-specified prior  $p(\theta)$ . If each individual-level posterior

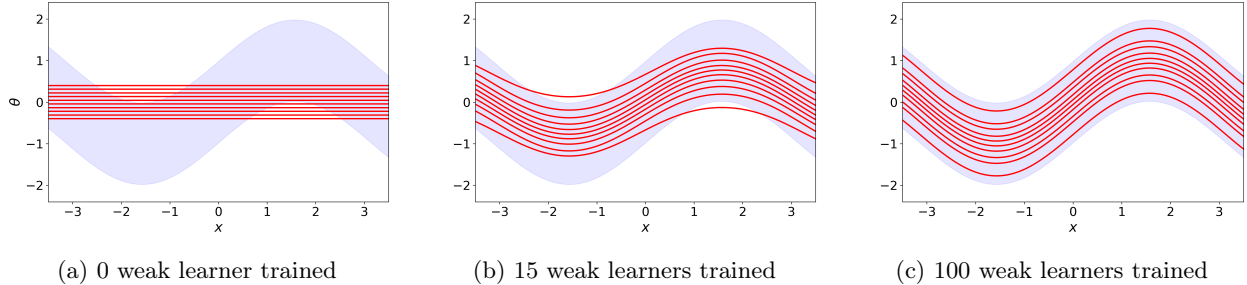


Figure 1: Illustration of inputs and outputs of WGBBoost trained on a training set  $\{x_i, \mu_i\}_{i=1}^{10}$  whose inputs are 10 grid points in  $[-3.5, 3.5]$  and output distributions are each a normal distribution  $\mu_i(\theta) = \mathcal{N}(\theta | \sin(x_i), 0.5)$  over  $\theta \in \mathbb{R}$ . The blue area indicates the 95% high probability region of the output distribution for each point. WGBBoost returns  $N$  particles (red lines) that predicts the output distribution for each input, where this illustration selects  $N = 10$  and uses a Gaussian kernel regressor as each weaker learner of WGBBoost.

falls into a closed form characterised by some hyperparameter, neural networks can be trained by using the hyperparameter of the individual-level posterior as a target value to predict for each input. Outstanding performance and computational efficiency of the existing approaches have been delivered in a wide spectrum of engineering and medical applications [16, 17, 18, 19]. However, the existing approaches are limited to neural networks and to the case where every individual-level posterior is in closed form so that the finite-dimensional hyperparameter can be predicted by proxy. In general, posterior distributions are known only up to their normalising constants and, therefore, require an approximation typically by particles [20].

Without closed-form expression, each individual-level posterior needs to be treated as an infinite-dimensional output for each input. This challenge poses the following fundamental question:

Consider supervised learning whose outputs are probability distributions. Given a training set of input values and output distributions  $\{x_i, \mu_i\}_{i=1}^D$ , can we build a model that receives an input  $x$  and returns a *nonparametric* prediction of the output distribution?

Motivated by this question, we formulate a general framework of Wasserstein gradient boosting (WGBBoost). WGBBoost receives an input and returns a particle-based prediction of the output probability distribution. Figure 1 illustrates inputs and outputs of WGBBoost. This paper considers application of WGBBoost to evidential learning, where the individual-level posterior  $p(\theta | y_i)$  of the response distribution  $p(y | \theta)$  is used as the output distribution  $\mu_i$  for each input  $x_i$  of the training set. Figure 2 compares the pipeline of evidential learning with Bayesian learning. To the author’s knowledge, WGBBoost is the first framework that enables evidential learning (i) for boosted tree models and (ii) without closed form of individual-level posteriors.

**Contributions** Our contributions are summarised as follows:

- Section 2 establishes the general framework of WGBBoost. It is a novel family of gradient boosting that returns a set of particles that approximates an output distribution assigned at each input. In contrast to standard gradient boosting that fits a weak learner to the gradient of a loss function, WGBBoost fits a weak learner to the estimated Wasserstein gradient of a loss functional over probability distributions.
- Section 3 establishes tree-based evidential learning based on WGBBoost, with the loss functional specified by the Kullback–Leibler (KL) divergence. Following modern gradient-boosting libraries [21, 22] that use second-order gradient boosting (c.f. Section 2.2), we use a second-order WGBBoost algorithm built on an approximate Wasserstein gradient and Hessian of the KL divergence (c.f. Sections 3.3 and 3.4).
- Section 4 demonstrates the performance of probabilistic regression and classification with OOD detection on real-world tabular datasets in comparison with common uncertainty quantification methods.

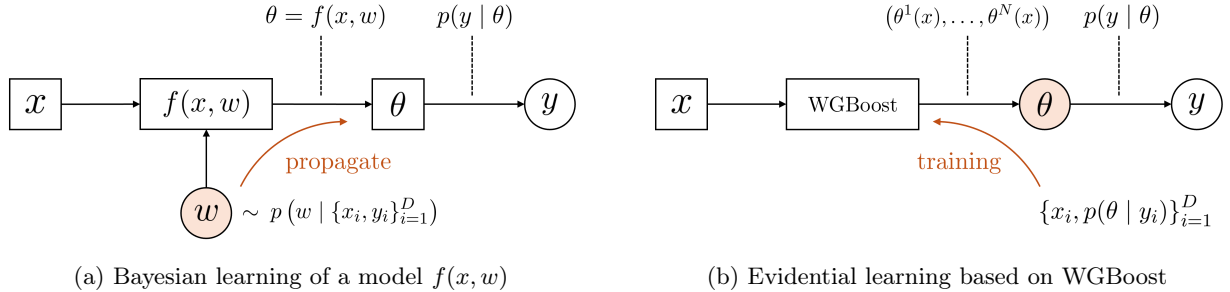


Figure 2: Comparison of the pipeline of (a) Bayesian learning and (b) evidential learning based on WGBBoost. The former uses the (global) posterior  $p(w | \{x_i, y_i\}_{i=1}^D)$  of the model parameter  $w$  conditional on all data, and samples multiple models from it. The latter uses the individual-level posterior  $p(\theta | y_i)$  of the response parameter  $\theta$  conditional on each individual datum  $y_i$  as the output distribution in the training set, and trains WGBBoost to directly returns a particle-based distributional estimate  $p(\theta | x)$  of  $\theta$  for each input  $x$ .

## 2 General Formulation of Wasserstein Gradient Boosting

This section presents the general formulation of WGBBoost. Section 2.1 recaps the notion of Wasserstein gradient flows, a ‘gradient’ system of probability distributions that minimises an objective functional in the Wasserstein space. Section 2.2 recaps the notion of gradient boosting, a sequential ensemble method that fits a new weak learner to the ‘gradient’ of the remaining loss at each iteration. Section 2.3 combines the above two notions to establish WGBBoost, a novel family of gradient boosting whose output is a set of particles that approximates an output distribution assigned at each input.

**Notation and Setting** Let  $\mathcal{X}$  and  $\mathcal{Y}$  denote the space of inputs and responses in classification and regression. Suppose  $\Theta = \mathbb{R}^d$ . Let  $\mathcal{P}_2$  be the 2-Wasserstein space, that is, a set of all probability distributions on  $\Theta$  with finite second moment equipped with the Wasserstein metric [23]. We identify a probability distribution in  $\mathcal{P}_2$  with its density whenever it exists. Denote by  $\odot$  and  $\oslash$ , respectively, elementwise multiplication and division of two vectors in  $\mathbb{R}^d$ . Let  $\nabla$  be the gradient operator. Let  $\nabla_{\mathbf{d}}^2$  be a second-order gradient operator that takes the second derivative at each coordinate i.e.  $\nabla_{\mathbf{d}}^2 f(\theta) = [\partial^2 f(\theta) / \partial \theta_1^2, \dots, \partial^2 f(\theta) / \partial \theta_d^2]^T \in \mathbb{R}^d$ .

### 2.1 Wasserstein Gradient Flow

In the Euclidean space, a gradient flow of a function  $f$  means a curve of points  $x_t$  that solves a differential equation  $(d/dt)x_t = -\nabla f(x_t)$  from an initial value  $x_0$ . That is the continuous-time limit of gradient descent, which minimises the function  $f$  as  $t \rightarrow \infty$ . A Wasserstein gradient flow means a curve of probability distributions  $\mu_t$  minimising a given functional  $\mathcal{F}$  on the 2-Wasserstein space  $\mathcal{P}_2$ . The Wasserstein gradient flow  $\mu_t$  is characterised as a solution of a partial differential equation, known as the *continuity equation*:

$$\frac{d}{dt} \mu_t = -\nabla \cdot (\mu_t \nabla_W \mathcal{F}(\mu_t)) \quad \text{given } \mu_0 \in \mathcal{P}_2, \quad (1)$$

where  $\nabla_W \mathcal{F}(\mu) : \Theta \rightarrow \Theta$  denotes the *Wasserstein gradient* of  $\mathcal{F}$  at  $\mu$  [24, 25]. Appendix A recaps the derivation of the Wasserstein gradient and presents the examples for several functionals.

One of the elegant properties of the Wasserstein gradient flow is casting the infinite-dimensional optimisation of the functional  $\mathcal{F}$  as a finite-dimensional particle update [23]. The continuity equation (1) can be reformulated as a dynamical system of a random variable  $\theta_t \sim \mu_t$ , such that

$$\frac{d}{dt} \theta_t = -[\nabla_W \mathcal{F}(\mu_t)](\theta_t) \quad \text{given } \theta_0 \sim \mu_0, \quad (2)$$

in the sense that the law  $\mu_t$  of the random variable  $\theta_t$  is a weak solution of the continuity equation. Consider the case where the initial measure  $\mu_0$  is set to the empirical distribution  $\hat{\mu}_0$  of  $N$  particles  $\{\theta_0^n\}_{n=1}^N$ . Discretising

the continuous-time system (2) by the Euler method with a small step size  $\nu > 0$  yields an iterative update scheme of  $N$  particles  $\{\theta_m^n\}_{n=1}^N$  from step  $m = 0$ :

$$\begin{bmatrix} \theta_{m+1}^1 \\ \vdots \\ \theta_{m+1}^N \end{bmatrix} = \begin{bmatrix} \theta_m^1 \\ \vdots \\ \theta_m^N \end{bmatrix} + \nu \begin{bmatrix} -[\nabla_W \mathcal{F}(\hat{\mu}_m)](\theta_m^1) \\ \vdots \\ -[\nabla_W \mathcal{F}(\hat{\mu}_m)](\theta_m^N) \end{bmatrix}, \quad (3)$$

where  $\hat{\mu}_m$  denotes the empirical distribution of the particles  $\{\theta_m^n\}_{n=1}^N$  at step  $m$ .

In practice, it is common that the Wasserstein gradient of a chosen functional  $\mathcal{F}$  is not well-defined for empirical distributions. In such cases, the particle update scheme (3) is not directly applicable because it depends on the Wasserstein gradient  $\nabla_W \mathcal{F}(\hat{\mu}_m)$  at the empirical distribution  $\hat{\mu}_m$ . For example, the KL divergence  $\mathcal{F}(\mu) = \text{KL}(\mu | \pi)$  with a reference distribution  $\pi$  has such a Wasserstein gradient  $[\nabla_W \mathcal{F}(\mu)](\theta) = -(\nabla \log \pi(\theta) - \nabla \log \mu(\theta))$  ill-defined when  $\mu$  is an empirical distribution. Hence, one often uses an estimate or approximation of the Wasserstein gradient of a functional  $\mathcal{F}$  that is well-defined for empirical distributions, in order to perform the particle update scheme (3) approximately [e.g. 26, 27, 28, 29, 30]. Our application of WGBost in Section 3 uses the ‘smoothed’ Wasserstein gradient of the KL divergence [26] recapped later.

## 2.2 Gradient Boosting

Gradient boosting [31] is a sequential ensemble method of  $M$  multiple weak learners  $f_1, \dots, f_M$ . It iteratively constructs an ensemble  $F_m$  of  $m$  weak learners  $f_1, \dots, f_m$  from step  $m = 0$  to  $M$ . Given the current ensemble  $F_m$  at step  $m$ , it trains a new weak learner  $f_{m+1}$  and constructs the next ensemble  $F_{m+1}$  by

$$F_{m+1}(x) = F_m(x) + \nu f_{m+1}(x) \quad (4)$$

where  $\nu$  is a shrinkage hyperparameter called a *learning rate*. The initial state of the ensemble  $F_0(x)$  at step  $m = 0$  is typically set to a constant that best fits the data. Any learning algorithm can be used as a weak learner in principle, although tree-based algorithms are most used [32].

The fundamental idea of gradient boosting is to train the new weak learner  $f_{m+1}$  to approximate the negative gradient of the remaining error of the current ensemble  $F_m$ . Suppose that outputs are vectors in  $\mathbb{R}^d$  and that a loss function  $L$  measures the remaining error at each data point  $R_i(F_m(x_i)) := L(F_m(x_i), y_i)$ . The new weak learner  $f_{m+1}$  is fitted to the set  $\{x_i, g_i\}_{i=1}^D$ , where the target variable  $g_i$  is specified as

$$g_i = -\nabla R_i(F_m(x_i)) \in \mathbb{R}^d.$$

The target variable  $g_i$  is often called a *pseudo residual*. At every fixed input  $x_i$ , the boosting scheme (4) updates the output of the current ensemble  $F_m(x_i)$  in the steepest descent direction of the error  $R_i(F_m(x_i))$ . Although [31] originally suggested performing an additional line search to determine a scaling constant for each weak learner, the line search has been reported to have a negligible influence on performance [33].

In modern gradient-boosting libraries such as XGBoost [21] and LightGBM [22], the standard practice is to use the diagonal (coordinatewise) Newton direction of the remaining error for the target variable of the new weak learner  $f_{m+1}$ . In this case, the new base learner  $f_{m+1}$  is fitted to the set  $\{x_i, g_i \oslash h_i\}_{i=1}^n$ , where the negative gradient  $g_i$  is divided elementwise by the Hessian diagonal  $h_i$  specified as

$$h_i = \nabla_d^2 R_i(F_m(x_i)) \in \mathbb{R}^d.$$

The target variable  $g_i \oslash h_i$  is the diagonal Newton direction that minimises the second-order Taylor approximation of the remaining error for each coordinate independently. Combining second-order gradient boosting with tree-based weak learners has demonstrated exceptional scalability and performance [34, 35]. Although it is possible to use the ‘full’ Newton direction as the target variable of each weak learner, the impracticality of the full Newton direction has been pointed out [e.g. 36, 37]. In addition, the coordinatewise computability of the diagonal Newton direction is suitable for popular gradient-boosting tree algorithms [36].

### 2.3 Wasserstein Gradient Boosting

Now we consider the setting of ‘distribution-valued’ supervised learning, where we are given a training set of input vectors and output distributions  $\{x_i, \mu_i\}_{i=1}^D \subset \mathcal{X} \times \mathcal{P}_2$ . Our goal is to construct a model that receives an input and returns a set of  $N$  particles whose empirical distribution approximates the output distribution. We specify a loss functional  $D(\cdot | \cdot)$  between two probability distributions—such as the KL divergence—to measure the remaining error  $\mathcal{F}_i(\cdot) = D(\cdot | \mu_i)$  of the model output for each  $i$ -th training output distribution  $\mu_i$ . Our idea is to combine gradient boosting with Wasserstein gradient, where we iteratively construct a set of  $N$  boosting ensembles  $F_m^1, \dots, F_m^N$ —each of which consists of  $m$  weak learners—from step  $m = 0$  to  $M$ .

Here, the output  $F_m^n(x)$  of each  $n$ -th boosting ensemble represents the  $n$ -th output particle for an input  $x$ . Given the current set of  $N$  ensembles  $F_m^1, \dots, F_m^N$  at step  $m$ , WGBBoost trains a set of  $N$  new weak learners  $f_{m+1}^1, \dots, f_{m+1}^N$  and computes the next set of  $N$  ensembles  $F_{m+1}^1, \dots, F_{m+1}^N$  by

$$\begin{bmatrix} F_{m+1}^1(x) \\ \vdots \\ F_{m+1}^N(x) \end{bmatrix} = \begin{bmatrix} F_m^1(x) \\ \vdots \\ F_m^N(x) \end{bmatrix} + \nu \begin{bmatrix} f_{m+1}^1(x) \\ \vdots \\ f_{m+1}^N(x) \end{bmatrix} \quad (5)$$

where  $\nu$  is a learning rate. Similarly to standard gradient boosting, we set the initial state of  $N$  ensembles  $F_0^1, \dots, F_0^N$  at step  $m = 0$  to a set of given constants. Throughout, denote by  $\hat{\mu}_{m,i}$  the empirical distribution of the  $N$  output particles  $F_m^1(x_i), \dots, F_m^N(x_i)$  for each  $i$ -th training input  $x_i$ .

As discussed in Section 2.1, the Wasserstein gradient often needs to be estimated when a distribution is an empirical distribution. For better presentation, let  $\mathcal{G}_i(\mu)$  denote an estimate of the Wasserstein gradient of the  $i$ -th remaining error  $\mathcal{F}_i(\mu)$  at arbitrary  $\mu$ . If the original Wasserstein gradient is well-defined for all  $\mu$ , it is a trivial estimate to use as  $\mathcal{G}_i(\mu)$ . Otherwise, any suitable estimate can be used as  $\mathcal{G}_i(\mu)$ . The fundamental idea of WGBBoost is to train the  $n$ -th new learner  $f_{m+1}^n$  to approximate the estimated Wasserstein gradient  $-\mathcal{G}_i(\hat{\mu}_{m,i})$  evaluated at the  $n$ -th boosting output  $F_m^n(x_i)$  for each  $x_i$ , so that,

$$\begin{bmatrix} f_{m+1}^1(x_i) \\ \vdots \\ f_{m+1}^N(x_i) \end{bmatrix} \approx \begin{bmatrix} -[\mathcal{G}_i(\hat{\mu}_{m,i})](F_m^1(x_i)) \\ \vdots \\ -[\mathcal{G}_i(\hat{\mu}_{m,i})](F_m^N(x_i)) \end{bmatrix}.$$

At every fixed  $x_i$ , the boosting scheme (5) approximates the particle update scheme (3) for the output particles  $F_m^1(x_i), \dots, F_m^N(x_i)$  under the estimated Wasserstein gradient  $\nabla_W \mathcal{F}_i(\hat{\mu}_{m,i})$ , by which each boosting output is updated in the direction to decrease the remaining error  $\mathcal{F}_i(\hat{\mu}_{m,i}) = D(\hat{\mu}_{m,i} | \mu_i)$  at step  $m$ .

The general procedure of WGBBoost is summarised in Algorithm 1. For our application, we focus on the KL divergence as a choice of the loss functional  $D(\cdot | \cdot)$  and use the Wasserstein gradient estimate based on kernel smoothing in Section 3. Appendix A presents examples of Wasserstein gradients of several divergences. Figure 1 illustrates the output of WGBBoost using a toy output distribution  $\mu_i(\cdot) = \mathcal{N}(\cdot | \sin(x_i), 0.5)$ .

**Remark 1 (Stochastic WGBBoost).** Stochastic gradient boosting [38] uses only a randomly sampled subset of data to fit a new weak learner at each step  $m$  to reduce the computational cost. The same subsampling approach can be applied for WGBBoost whenever the dataset is large.

**Remark 2 (Second-Order WGBBoost).** If an estimate of the Wasserstein ‘Hessian’ of the remaining error  $\mathcal{F}_i$  is available, the Newton direction of  $\mathcal{F}_i$  may also be computable [e.g. 39, 40]. We can immediately implement a second-order WGBBoost algorithm by plugging such a Newton direction into  $\mathcal{G}_i(\mu)$  in Algorithm 1. Our default WGBBoost algorithm for tree-based evidential learning is built on a diagonal approximate Newton direction of the KL divergence, aligning with the standard practice in modern gradient-boosting libraries to use the diagonal Newton direction.

---

**Algorithm 1:** Wasserstein Gradient Boosting

---

**Input:** training set  $\{x_i, \mu_i\}_{i=1}^D$  of input  $x_i \in \mathcal{X}$  and output distribution  $\mu_i \in \mathcal{P}_2$

**Parameter:** loss functional  $D(\cdot | \cdot)$ , estimate  $\mathcal{G}_i(\mu)$  of the Wasserstein gradient of  $D(\mu | \mu_i)$ , particle number  $N$ , iteration  $M$ , learning rate  $\nu$ , weak learner  $f$ , initial constants  $(\vartheta_0^1, \dots, \vartheta_0^N)$

**Output:** set of  $N$  boosting ensembles  $(F_M^1, \dots, F_M^N)$  at final step  $M$

$(F_0^1(\cdot), \dots, F_0^N(\cdot)) \leftarrow (\vartheta_0^1, \dots, \vartheta_0^N)$   $\triangleright$  set initial state of  $N$  boosting ensembles

**for**  $m \leftarrow 0, \dots, M - 1$  **do**

**for**  $i \leftarrow 1, \dots, D$  **do**

$\hat{\mu}_{m,i} \leftarrow$  empirical distribution of set of  $N$  output values  $(F_m^1(x_i), \dots, F_m^N(x_i))$  for input  $x_i$

**for**  $n \leftarrow 1, \dots, N$  **do**

$g_i^n \leftarrow -[\mathcal{G}_i(\hat{\mu}_{m,i})](F_m^n(x_i))$   $\triangleright$  Wasserstein gradient evaluated at  $n$ -th output value for  $x_i$

**end**

**end**

**for**  $n \leftarrow 1, \dots, N$  **do**

$f_{m+1}^n \leftarrow$  fit  $(\{x_i, g_i^n\}_{i=1}^D)$   $\triangleright$  fit  $n$ -th new weak learner to Wasserstein gradients

$F_{m+1}^n(\cdot) \leftarrow F_m^n(\cdot) + \nu f_{m+1}^n(\cdot)$   $\triangleright$  get next state of  $n$ -th boosting ensemble

**end**

**end**

---

### 3 Default Setting for Tree-Based Evidential Learning

This section provides the default setting to implement a concrete WBoost algorithm for evidential learning, which enables classification and regression with predictive uncertainty. The individual-level posterior  $p(\theta | y_i)$  of a response distribution  $p(y | \theta)$  is used as the output distribution  $\mu_i$  in the training set  $\{x_i, \mu_i\}_{i=1}^D$  of WBoost. Section 3.1 recaps derivation of the individual-level posterior  $p(\theta | y_i)$ , followed by the default choice of the prior discussed in Section 3.2. We choose the KL divergence as a loss functional  $D(\cdot | \cdot)$  of WBoost. Section 3.3 recaps a widely-used approximation of the Wasserstein gradient of the KL divergence based on kernel smoothing [26]. A further advantage of the kernel smoothing approach is that the approximate Wasserstein Hessian is available, with which Section 3.4 establishes a second-order WBoost algorithm similarly to modern gradient-boosting libraries.

#### 3.1 Individual-Level Posteriors as Output Distributions

Suppose that a response distribution  $p(y | \theta)$  is specified for a response variable  $y$  of one's classification or regression problem, as is typically done. Suppose further that a prior distribution  $p_i(\theta)$  of the response parameter  $\theta$  is specified at each individual observed input  $x_i$ . At each individual observation  $(x_i, y_i)$ , the response-distribution likelihood  $p(y_i | \theta)$  and the prior  $p_i(\theta)$  determine the individual-level posterior

$$p(\theta | y_i) \propto p(y_i | \theta)p_i(\theta).$$

The individual-level posterior is used as the output distribution  $\mu_i$  for each input  $x_i$  in the training set  $\{x_i, \mu_i\}_{i=1}^D$  of WBoost. We apply the framework of WBoost to construct a model that returns a set of particles that approximates the output distribution  $\mu_i(\cdot) = p(\cdot | y_i)$  for each observed input  $x_i$ .

For a new input  $x$ , the trained WBoost model returns a set of particles  $(\theta^1(x), \dots, \theta^N(x))$  that is a nonparametric distributional estimate  $p(\theta | x)$  of the response parameter. Based on the output particles, a predictive distribution  $p(y | x)$  of the response  $y$  for each new input  $x$  can be defined via marginalisation:

$$p(y | x) = \int_{\Theta} p(y | \theta)p(\theta | x)d\theta = \frac{1}{N} \sum_{i=1}^N p(y | \theta^i(x)). \quad (6)$$

A point prediction  $\hat{y}$  for each new input  $x$  can also be defined via the ‘individual-level’ Bayes action:

$$\hat{y} = \operatorname{argmin}_{y \in \mathcal{Y}} \int_{\Theta} U(y, \theta) p(\theta | x) d\theta = \operatorname{argmin}_{y \in \mathcal{Y}} \frac{1}{N} \sum_{i=1}^N U(y, \theta^i(x)),$$

which is the minimiser of the average risk of a given utility  $U : \mathcal{Y} \times \Theta \rightarrow \mathbb{R}$ . For example, if the utility is a quadratic function  $U(y, \theta) = (y - \theta)^2$ , the Bayes action is the mean of the output particles  $(\theta^1(x), \dots, \theta^N(x))$ .

In general, the explicit form of the individual-level posterior  $p(\theta | y_i)$  is known only up to the normalising constant. The WGBoost algorithm for evidential learning, provided in Section 3.4, requires no normalising constant of the individual-level posterior  $p(\theta | y_i)$ . It depends only on the log-gradient of the individual-level posterior  $\nabla \log p(\theta | y_i) = \nabla p(\theta | y_i) / p(\theta | y_i)$ , cancelling the normalising constant by fraction. Hence, knowing the form of the response-distribution likelihood  $p(y_i | \theta)$  and the prior  $p_i(\theta)$  suffices.

**Remark 3 (Difference from Bayesian Learning).** Bayesian learning of a given model  $f(x, w)$  uses the posterior  $p(w | \{x_i, y_i\}_{i=1}^D)$  of the model parameter  $w$  conditional on all data. The predictive distribution  $p(y | x)$  of the response  $y$  in Bayesian learning is defined via marginalisation of the model parameter  $w$ , that is,  $p(y | x) = \int_{\Theta} p(y | \theta = f(x, w)) p(w | \{x_i, y_i\}_{i=1}^D) dw$ . In contrast, WGBoost learns the nonparametric distributional estimate  $p(\theta | x)$  directly from the training set  $\{x_i, \mu_i\}_{i=1}^D$ , involving no marginalisation of the model parameter  $w$  that is often exceedingly high dimensional in machine learning.

### 3.2 Choice of Individual-Level Priors

The prior  $p_i(\theta)$  of the response parameter  $\theta$  is specified at each individual observed input  $x_i$ . The approach to specifying the prior may differ depending on whether past data are available. When past data are available, past data can be utilised in any possible way to elicit a reasonable prior for future data. When no past data are available, we recommend the use of a noninformative prior that have been developed as a sensible choice of prior in the absence of past data; see [e.g. 41] for the introduction. To avoid numerical errors, if a noninformative prior is improper (nonintegrable) as is often the case, we recommend the use of a proper probability distribution that approximates the noninformative prior sufficiently well.

**Example 1 (Normal Location-Scale).** Consider regression with a scalar-valued response variable  $y \in \mathbb{R}$ . A normal location-scale distribution  $\mathcal{N}(y | m, \sigma)$  has the mean and scale parameters  $m \in \mathbb{R}$  and  $\sigma \in (0, \infty)$ . A typical noninformative prior of  $m$  and  $\sigma$  are given by 1 and  $1/\sigma$  respectively, which are improper. At every observation  $(x_i, y_i)$ , we use a normal prior  $\mathcal{N}(m | 0, \sigma_0)$  over  $m$  and an inverse gamma prior  $\text{IG}(\sigma | \alpha_0, \beta_0)$  over  $\sigma$ , with the hyperparameters  $\sigma_0 = 10$  and  $\alpha_0 = \beta_0 = 0.01$ , which approximate the non-informative priors.

**Example 2 (Categorical).** Consider classification with a  $k$ -class label response variable  $y \in \{1, \dots, k\}$ . A categorical distribution  $\mathcal{C}(y | q)$  has a class probability parameter  $q = (q_1, \dots, q_k)$  in the  $k$ -dimensional simplex  $\Delta_k$ . If  $k = 2$ , it corresponds to the Bernoulli distribution. A typical noninformative prior of  $q$  is given by  $1 / \prod_{i=1}^k q_i$ . At every observation  $(x_i, y_i)$ , we use the logistic normal prior—a multivariate generalisation of the logit normal distribution [42]—over  $q$  with the mean 0 and identity covariance matrix scaled by 10.

In Section 2, we have supposed that  $\Theta = \mathbb{R}^d$  for some dimension  $d$ . Any parameter that lies in a subset of the Euclidean space (e.g.  $\sigma$ ) can be reparametrised as one in the Euclidean space (e.g.  $\log \sigma$ ). Appendix D details the reparametrisation used for the experiment. If a dataset has scalar outputs and they have a low or high order of magnitude, we also recommend standardising the outputs to adjust the magnitude.

### 3.3 Approximate Wasserstein Gradient of KL Divergence

The loss functional  $D(\mu | \mu_i)$  considered in this setting is the KL divergence  $\text{KL}(\mu | \mu_i)$ . A computational challenge of the KL divergence is that the associated Wasserstein gradient  $[\mathcal{G}_i^{\text{KL}}(\mu)](\theta) := -(\nabla \log \pi_i(\theta) - \nabla \log \mu(\theta))$  is not well-defined for empirical distributions. A particularly successful approach to finding a well-defined approximation of the Wasserstein gradient—which originates in [43] and has been

applied in wide contexts [26, 44, 45]—is to smooth the original Wasserstein gradient through a kernel integral operator  $\int_{\Theta} [\mathcal{G}_i^{\text{KL}}(\mu)](\theta^*) k(\theta, \theta^*) d\mu(\theta^*)$  [46]. By integration-by-part (see [e.g. 43]), the smoothed Wasserstein gradient—denoted  $\mathcal{G}_i^*(\mu)$ —falls into the following form that is well-defined for any distribution  $\mu$ :

$$[\mathcal{G}_i^*(\mu)](\theta) := -\mathbb{E}_{\theta^* \sim \mu} \left[ \nabla \log \mu_i(\theta^*) k(\theta, \theta^*) + \nabla k(\theta, \theta^*) \right] \in \mathbb{R}^d, \quad (7)$$

where  $\nabla k(\theta, \theta^*)$  denotes the gradient of  $k$  with respect to the first argument  $\theta$ . An approximate Wasserstein gradient flow based on the smoothed Wasserstein gradient  $\mathcal{G}_i^*(\mu)$  is called the Stein variational gradient descent [43] or kernelised Wasserstein gradient flow [47]. In most cases, the kernel  $k$  is set to the Gaussian kernel  $k(\theta, \theta^*) = \exp(-\|\theta - \theta^*\|^2/h)$  with the scale hyperparameter  $h > 0$ . We use the Gaussian kernel with the scale hyperparameter  $h = 0.1$  throughout this work.

Another common approach to approximating the Wasserstein gradient flow of the KL divergence is the Langevin diffusion approach [48]. The discretised algorithm, called the unadjusted Langevin algorithm [49], is a stochastic particle update scheme that adds a Gaussian noise at every iteration. However, several known challenges, such as asymptotic bias and slow convergence, often necessitate an ad-hoc adjustment of the algorithm [48]. Appendix B discusses a variant of WGBost built on the Langevin algorithm, although it is not considered the default implementation.

### 3.4 Second-Order Implementation of WGBost

Following the standard practice in modern gradient-boosting libraries [21, 22] to use the diagonal Newton direction, we further consider a diagonal (coordinatewise) approximate Wasserstein Newton direction of the KL divergence. In a similar manner to the smoothed Wasserstein gradient (7), the approximate Wasserstein Hessian of each KL divergence  $\text{KL}(\mu \mid \mu_i)$  can be obtained by the kernel smoothing. The diagonal of the approximate Wasserstein Hessian, denoted  $\mathcal{H}_i^*(\mu)$ , is defined by

$$[\mathcal{H}_i^*(\mu)](\theta) := \mathbb{E}_{\theta^* \sim \mu} \left[ -\nabla_{\text{d}}^2 \log \mu_i(\theta^*) k(\theta, \theta^*)^2 + \nabla k(\theta, \theta^*) \odot \nabla k(\theta, \theta^*) \right] \in \mathbb{R}^d. \quad (8)$$

The diagonal approximate Wasserstein Newton direction of each KL divergence is then defined by  $-\mathcal{G}_i^*(\mu)(\cdot) \odot [\mathcal{H}_i^*(\mu)](\cdot)$ . Appendix C provides the derivation based on [39] who derived the Newton direction of the KL divergence in the context of nonparametric variational inference. The second-order WGBost algorithm is established by plugging it into  $\mathcal{G}_i(\mu)$  in Algorithm 1 i.e. setting

$$[\mathcal{G}_i(\mu)](\cdot) = [\mathcal{G}_i^*(\mu)](\cdot) \odot [\mathcal{H}_i^*(\mu)](\cdot). \quad (9)$$

Algorithm 1 under the setting (9) is considered our default WGBost algorithm for evidential learning. We refer this algorithm to as the *Wasserstein-boosted evidential learning* (WEvidential). The explicit pseudocode is provided in Algorithm 2 for full clarity.

**Remark 4 (Computation).** The diagonal Newton direction has a clear computational benefit in that only elementwise division is involved. The computational complexity is the same as that for the smoothed Wasserstein gradient, scaling linearly to both the particle number  $N$  and the particle dimension  $d$ . Hence, there is essentially *no reason not to use* the diagonal Newton direction instead of the smoothed Wasserstein gradient. Although it is possible to use the full Newton direction with no diagonal approximation, the inverse and product of  $(N \times d) \times (N \times d)$  matrices are required at every computation of the direction (c.f. Appendix D). Appendix D presents a simulation study to compare computational time and convergence speed of WGBost algorithms implemented with four different estimates of the Wasserstein gradient.

## 4 Applications with Real-world Tabular Data

We empirically demonstrate the performance of the WGBost algorithm through three applications using real-world tabular data. The first application illustrates the output of WGBost through a simple conditional



---

**Algorithm 2:** Wasserstein-Boosted Evidential Learning

---

**Input:** dataset  $\{x_i, y_i\}_{i=1}^D$  of input  $x_i$  and response  $y_i$  of classification or regression  
**Parameter:** individual-level posterior  $p(\theta | y_i)$  of response distribution  $p(y | \theta)$  conditional on each  $y_i$ , particle number  $N$ , iteration  $M$ , learning rate  $\nu$ , weak learner  $f$ , initial constants  $\{\vartheta_0^n\}_{n=1}^N$   
**Output:** set of  $N$  boosting ensembles  $(F_M^1, \dots, F_M^N)$  at final step  $M$   
 $(F_0^1(\cdot), \dots, F_0^N(\cdot)) \leftarrow (\vartheta_0^1, \dots, \vartheta_0^N)$   $\triangleright$  set initial state of  $N$  boostings  
**for**  $m \leftarrow 0, \dots, M - 1$  **do**  
  **for**  $i \leftarrow 1, \dots, D$  **do**  
     $\hat{\mu}_{m,i} \leftarrow$  empirical distribution of set of  $N$  output values  $(F_m^1(x_i), \dots, F_m^N(x_i))$  for input  $x_i$   
    **for**  $n \leftarrow 1, \dots, N$  **do**  
       $g_i^n \leftarrow \mathbb{E}_{\theta^* \sim \hat{\mu}_{m,i}} [\nabla \log p(\theta^* | y_i) k(F_m^n(x_i), \theta^*) + \nabla k(F_m^n(x_i), \theta^*)]$   
       $h_i^n \leftarrow \mathbb{E}_{\theta^* \sim \hat{\mu}_{m,i}} [-\nabla_{\mathbf{d}}^2 \log p(\theta^* | y_i) k(F_m^n(x_i), \theta^*)^2 + \nabla k(F_m^n(x_i), \theta^*) \odot \nabla k(F_m^n(x_i), \theta^*)]$   
    **end**  
  **end**  
  **for**  $n \leftarrow 1, \dots, N$  **do**  
     $f_{m+1}^n \leftarrow$  fit  $(\{x_i, g_i^n \odot h_i^n\}_{i=1}^D)$   $\triangleright$  fit  $n$ -th new tree regressor to approximate Newton directions  
     $F_{m+1}^n(\cdot) \leftarrow F_m^n(\cdot) + \nu f_{m+1}^n(\cdot)$   $\triangleright$  set next state of  $n$ -th boosting  
  **end**  
**end**

---

density estimation. The second application benchmarks the regression performance on nine real-world datasets [50]. The third application examines the classification and OOD detection performance on the real-world datasets used in [14]. The source code is available in <https://github.com/takuomatsubara/WGBoost>.

**Common Hyperparameters:** Throughout, we set the number of output particles  $N$  to 10 and set each weak learner  $f$  to the decision tree regressor [51] with maximum depth 1 for the first application and 3 for the rest. We set the learning rate  $\nu$  to 0.1 for regression and 0.4 for classification. Appendix E contains further details, including a choice of the initial constant  $\{\vartheta_0^n\}_{n=1}^N$ .

## 4.1 Illustrative Conditional Density Estimation

This section illustrates the output of the WGBoost algorithm by estimating a conditional density  $p(y | x)$  from one-dimensional scalar inputs and outputs  $\{x_i, y_i\}_{i=1}^D$ . The normal output distribution  $\mathcal{N}(y | m, \sigma)$  and the prior  $p_i(m, \sigma)$  in Example 1 were used to define the individual-level posterior  $p(m, \sigma | y_i)$ , in which case the output of the WGBoost algorithm is a set of 10 particles  $\{(m^n(x), \sigma^n(x))\}_{n=1}^{10}$  of the mean and scale parameters for each input  $x$ . We set the number of weak learners  $M$  to 500.

The conditional density is estimated using the predictive distribution (6) by the WGBoost algorithm. We used two real-world datasets, *bone mineral density* [52] and *old faithful geyser* [53]. Figure 3 depicts the result for the former dataset, demonstrating that the WGBoost algorithm captures the heterogeneity of the conditional density on each input well. Similarly, Figure 4 depicts the result for the latter dataset.

## 4.2 Probabilistic Regression Benchmark

This section examines the regression performance of the WGBoost algorithm using a standard benchmark protocol that originated in [50] and has been used in a number of subsequent works [10, 9, 32]. The benchmark protocol uses real-world tabular datasets from the UCI machine learning repository [54], each with one-dimensional scalar responses. As in Section 4.1, the normal response distribution  $\mathcal{N}(y | m, \sigma)$  and the prior  $p_i(m, \sigma)$  in Example 1 were used to define the individual-level posterior  $p(m, \sigma | y_i)$ .

We randomly held out 10% of each dataset as a test set, following the data splitting protocol in [50]. The

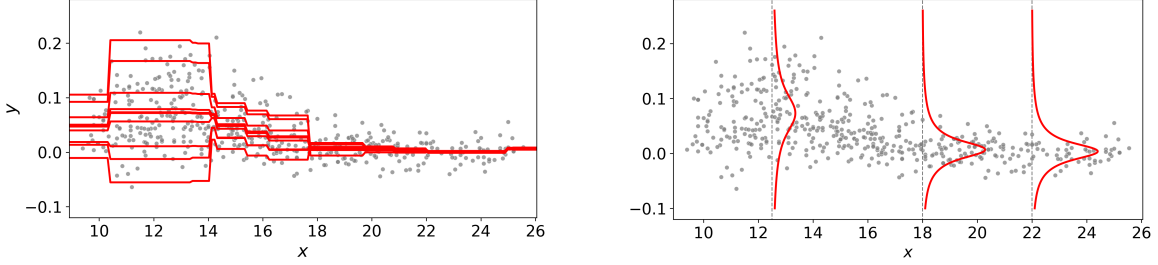


Figure 3: Conditional density estimation for the bone mineral density dataset (grey dots) by WEvidential, where the normal response distribution  $\mathcal{N}(y | m, \sigma)$  is specified for the response variable  $y$ . Left: distributional estimate (10 particles) of the location parameter  $\{m^n(x)\}_{n=1}^{10}$  for each input. Right: estimated density (6) based on the normal response distribution averaged over the output particles  $\{(m^n(x), \sigma^n(x))\}_{n=1}^{10}$ .

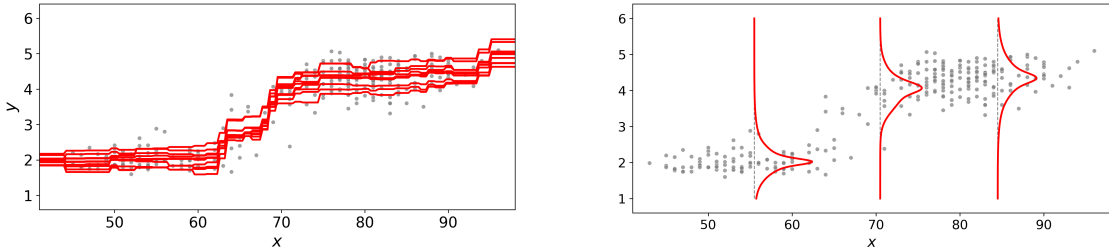


Figure 4: Conditional density estimation for the old faithful geyser dataset (grey dots) by WEvidential. Left: distributional estimate (10 particles) of the location parameter for each input. Right: estimated density by the predictive distribution (6) based on the output particles.

negative log likelihood (NLL) is measured by using the predictive distribution (6) by the WGBost algorithm. The room mean squared error (RMSE) is measured by using the point prediction produced by taking the mean value of the predictive distribution. For this benchmark, we followed an approach used in [32] to choose the number of weak learners  $M$  by early-stopping, where we held out 20% of the training set as a validation set to choose the number  $1 \leq M \leq 4000$  achieving the least validation error. Once the number  $M$  was chosen, the WGBost algorithm was trained again using all the entire training set. We repeated this procedure 20 times for each dataset, except the *protein* dataset for which we repeated five times.

We compared the performance of WEvidential with five other methods: Monte Carlo Dropout (MCDropout) [9], Deep Ensemble (DEnsemble) [10], Concrete Dropout (CDropout) [55], Natural Gradient Boosting (NGBoost) [32], and Deep Evidential Regression (DEvidential) [13]. Appendix E briefly describes each algorithm and provides further details on the experiment. Table 1 summarises the NLLs and RMSEs of the six algorithms. The WGBost algorithm achieves the best score or a score sufficiently close to the best score for the majority of the datasets.

### 4.3 Classification and Out-of-Distribution Detection

This section examines the classification and anomaly OOD detection performance of the WGBost algorithm on two real-world tabular datasets, *segment* and *sensorless*, following the protocol used in [14]. The categorical output distribution  $\mathcal{C}(y | q)$  and the prior  $p_i(q)$  in Example 2 were used to define the individual-level posterior  $p(q | y_i)$ , in which case the output of the WGBost algorithm is a set of 10 particles  $\{q^n\}_{n=1}^{10}$  of the class probability parameter  $q$  in the simplex  $\Delta^k$  for each input  $x$ . We set the number of weak learners  $M$  to 4000. The dispersion of the output particles of the WGBost algorithm was used for OOD detection [56]. If a test input was an *in-distribution* sample from the same distribution as the data, we expected the output particles

Table 1: The NLLs and RMSEs with the standard deviation. The best score is underlined for each dataset, and the scores whose standard deviation ranges include the best score are in bold. Results of MCDropout, DEnsembles, CDropout, NGBoost, and DEvidential were reported in [9], [10], [55], [32] and [13] respectively.

Dataset	Criteria	WEvidential	MCDropout	DEnsemble	CDropout	NGBoost	DEvidential
boston		<b>2.47 ± 0.16</b>	2.46 ± 0.06	<b>2.41 ± 0.25</b>	2.72 ± 0.01	<b>2.43 ± 0.15</b>	<b>2.35 ± 0.06</b>
concrete		<b>2.83 ± 0.11</b>	3.04 ± 0.02	3.06 ± 0.18	3.51 ± 0.00	3.04 ± 0.17	3.01 ± 0.02
energy		<b>0.53 ± 0.08</b>	1.99 ± 0.02	1.38 ± 0.22	2.30 ± 0.00	<b>0.60 ± 0.45</b>	1.39 ± 0.06
kin8nm		-0.44 ± 0.03	-0.95 ± 0.01	-1.20 ± 0.02	-0.65 ± 0.00	-0.49 ± 0.02	<b>-1.24 ± 0.01</b>
naval	NLL	-5.47 ± 0.03	-3.80 ± 0.01	-5.63 ± 0.05	<b>-5.87 ± 0.05</b>	-5.34 ± 0.04	-5.73 ± 0.07
power		<b>2.60 ± 0.04</b>	2.80 ± 0.01	2.79 ± 0.04	2.75 ± 0.01	2.79 ± 0.11	2.81 ± 0.07
protein		2.70 ± 0.01	2.89 ± 0.00	2.83 ± 0.02	2.81 ± 0.00	2.81 ± 0.03	<b>2.63 ± 0.00</b>
wine		<b>0.95 ± 0.08</b>	0.93 ± 0.01	<b>0.94 ± 0.12</b>	1.70 ± 0.00	<b>0.91 ± 0.06</b>	<b>0.89 ± 0.05</b>
yacht		<b>0.16 ± 0.24</b>	1.55 ± 0.03	1.18 ± 0.21	1.75 ± 0.00	<b>0.20 ± 0.26</b>	1.03 ± 0.19
boston		<b>2.78 ± 0.60</b>	2.97 ± 0.19	<b>3.28 ± 1.00</b>	<b>2.65 ± 0.17</b>	<b>2.94 ± 0.53</b>	3.06 ± 0.16
concrete		<b>4.15 ± 0.52</b>	5.23 ± 0.12	6.03 ± 0.58	4.46 ± 0.16	5.06 ± 0.61	5.85 ± 0.15
energy		<b>0.42 ± 0.07</b>	1.66 ± 0.04	2.09 ± 0.29	0.46 ± 0.02	<b>0.46 ± 0.06</b>	2.06 ± 0.10
kin8nm		0.15 ± 0.00	0.10 ± 0.00	0.09 ± 0.00	<b>0.07 ± 0.00</b>	0.16 ± 0.00	0.09 ± 0.00
naval	RMSE	<b>0.00 ± 0.00</b>	0.01 ± 0.00	<b>0.00 ± 0.00</b>	<b>0.00 ± 0.00</b>	<b>0.00 ± 0.00</b>	<b>0.00 ± 0.00</b>
power		<b>3.19 ± 0.25</b>	4.02 ± 0.04	4.11 ± 0.17	3.70 ± 0.04	3.79 ± 0.18	4.23 ± 0.09
protein		4.09 ± 0.02	4.36 ± 0.01	4.71 ± 0.06	<b>3.85 ± 0.02</b>	4.33 ± 0.03	4.64 ± 0.03
wine		<b>0.61 ± 0.05</b>	<b>0.62 ± 0.01</b>	<b>0.64 ± 0.04</b>	0.62 ± 0.00	<b>0.63 ± 0.04</b>	<b>0.61 ± 0.02</b>
yacht		<b>0.48 ± 0.18</b>	1.11 ± 0.09	1.58 ± 0.48	0.57 ± 0.05	<b>0.50 ± 0.20</b>	1.57 ± 0.56

to concentrate on some small region in  $\Delta^k$  indicating a high probability of the correct class. If a test input was an OOD sample, we expected the output particles to disperse over  $\Delta^k$  because the model ought to be less certain about the correct class.

The segment and sensorless datasets have 7 and 11 classes in total. For the segment dataset, the data subset that belongs to the last class was kept as the OOD samples. For the sensorless dataset, the data subset that belongs to the last two classes was kept as the OOD samples. For each dataset, 20% of the non-OOD samples is held out as a test set to measure the classification accuracy. Several approaches can define the OOD score of each input [56]. We focused on an approach that uses the variance of the output particles as the OOD score. For the WGBBoost algorithm, we employed the inverse of the maximum norm of the variance as the OOD score. Given the OOD score, we measured the OOD detection performance by the area under the precision recall curve (PR-AUC), viewing non-OOD test data as the positive class and OOD data as the negative class. We repeated this procedure five times.

We compared the WGBBoost algorithm with four other methods: MCDropout, DEnsemble, and Distributional Distillation (DDistillation) [57], and Posterior Network (PNetwork) [14]. Appendix E briefly describes each algorithm and provides further details on the experiment. Table 2 summarises the classification and OOD detection performance of the five algorithms. The WGBBoost algorithm demonstrates a high classification and

Table 2: The classification accuracies and OOD detection PR-AUCs with the standard deviation. For each dataset, the best score is underlined and in bold. The results other than WEvidential were reported in [14].

Dataset	Criteria	WEvidential	MCDropout	DEnsemble	DDistillation	PNetwork
segment	Accuracy	96.57 ± 0.6	95.25 ± 0.1	<b>97.27 ± 0.1</b>	96.21 ± 0.1	96.92 ± 0.1
	OOD	<b>99.67 ± 0.2</b>	43.11 ± 0.6	58.13 ± 1.7	35.83 ± 0.4	96.74 ± 0.9
sensorless	Accuracy	<b>99.54 ± 0.1</b>	89.32 ± 0.2	99.37 ± 0.0	93.66 ± 1.5	99.52 ± 0.0
	OOD	81.13 ± 5.3	40.61 ± 0.7	50.62 ± 0.1	31.17 ± 0.2	<b>88.65 ± 0.4</b>

OOD detection accuracy simultaneously. Although PNetwork has the best OOD detection performance for the sensorless dataset, the performance of the WGBost algorithm also exceeds 80%, which is distinct from MCDropout, DEnsemble, and DDistillation.

## 5 Discussion

This work established the general framework of WGBost for 'distribution-valued' supervised learning, which receives a particle-based approximation of an output distribution assigned at each input. We focused on application of WGBost to evidential learning, for which we provided the setting to implement a second-order WGBost algorithm, aligning with the standard practice in modern gradient-boosting libraries. We empirically demonstrated that the probabilistic forecast by WGBost leads to better predictive accuracy and OOD detection performance.

The established framework of WGBost offers exciting avenues for future research. Important directions for future study include (i) investigating the convergence properties, (ii) evaluating the robustness to misspecified response distributions, and (iii) exploring alternative loss functionals to the KL divergence. A limitation of WGBost may arise when data are not tabular, as in the case of standard gradient boosting. These questions require careful examination and are critical for future work.

## References

- [1] Ravid Shwartz-Ziv and Amitai Armon. Tabular data: Deep learning is not all you need. *Information Fusion*, 81:84–90, 2022.
- [2] Moloud Abdar, Farhad Pourpanah, Sadiq Hussain, Dana Rezazadegan, Li Liu, Mohammad Ghavamzadeh, Paul Fieguth, Xiaochun Cao, Abbas Khosravi, U. Rajendra Acharya, Vladimir Makarenkov, and Saeid Nahavandi. A review of uncertainty quantification in deep learning: Techniques, applications and challenges. *Information Fusion*, 76:243–297, 2021.
- [3] Eric Topol. High-performance medicine: the convergence of human and artificial intelligence. *Nature Medicine*, 25:44–56, 2019.
- [4] Sorin Grigorescu, Bogdan Trasnea, Tiberiu Cocias, and Gigel Macesanu. A survey of deep learning techniques for autonomous driving. *Journal of Field Robotics*, 37(3):362–386, 2020.
- [5] Matthew Richardson, Ewa Dominowska, and Robert Ragno. Predicting clicks: estimating the click-through rate for new ads. In *Proceedings of the 16th International Conference on World Wide Web*, page 521–530, 2007.
- [6] Christopher Burges. From ranknet to lambdarank to lambdamart: An overview. *Learning*, 11, 2010.
- [7] Byron P. Roe, Hai-Jun Yang, Ji Zhu, Yong Liu, Ion Stancu, and Gordon McGregor. Boosted decision trees as an alternative to artificial neural networks for particle identification. *Nuclear Instruments and Methods in Physics Research Section A: Accelerators, Spectrometers, Detectors and Associated Equipment*, 543(2):577–584, 2005.
- [8] James Bennett and Stan Lanning. The Netflix prize. In *Proceedings of the KDD Cup Workshop 2007*, pages 3–6, 2007.
- [9] Yariv Gal and Zoubin Ghahramani. Dropout as a Bayesian approximation: Representing model uncertainty in deep learning. In *Proceedings of The 33rd International Conference on Machine Learning*, volume 48 of *Proceedings of Machine Learning Research*, pages 1050–1059. PMLR, 2016.
- [10] Balaji Lakshminarayanan, Alexander Pritzel, and Charles Blundell. Simple and scalable predictive uncertainty estimation using deep ensembles. In *Advances in Neural Information Processing Systems*, volume 30, 2017.

- [11] Murat Sensoy, Lance Kaplan, and Melih Kandemir. Evidential deep learning to quantify classification uncertainty. In *Advances in Neural Information Processing Systems*, volume 31, 2018.
- [12] Jakob Gawlikowski, Cedrique Rovile Njjeutcheu Tassi, Mohsin Ali, Jongseok Lee, Matthias Humt, Jianxiang Feng, Anna Kruspe, Rudolph Triebel, Peter Jung, Ribana Roscher, Muhammad Shahzad, Wen Yang, Richard Bamler, and Xiao Xiang Zhu. A survey of uncertainty in deep neural networks. *Artificial Intelligence Review*, 56:1513–1589, 2023.
- [13] Alexander Amini, Wilko Schwarting, Ava Soleimany, and Daniela Rus. Deep evidential regression. In *Advances in Neural Information Processing Systems*, volume 33, pages 14927–14937, 2020.
- [14] Bertrand Charpentier, Daniel Zügner, and Stephan Günnemann. Posterior network: Uncertainty estimation without OOD samples via density-based pseudo-counts. In *Advances in Neural Information Processing Systems*, volume 33, pages 1356–1367. Curran Associates, Inc., 2020.
- [15] Dennis Thomas Ulmer, Christian Hardmeier, and Jes Frellesen. Prior and posterior networks: A survey on evidential deep learning methods for uncertainty estimation. *Transactions on Machine Learning Research*, 2023.
- [16] Edouard Capellier, Franck Davoine, Veronique Cherfaoui, and You Li. Evidential deep learning for arbitrary lidar object classification in the context of autonomous driving. In *2019 IEEE Intelligent Vehicles Symposium (IV)*, pages 1304–1311, 2019.
- [17] Patrick Hemmer, Niklas Kühl, and Jakob Schöffner. Deal: Deep evidential active learning for image classification. In *2020 19th IEEE International Conference on Machine Learning and Applications (ICMLA)*, pages 865–870, 2020.
- [18] Ava P. Soleimany, Alexander Amini, Samuel Goldman, Daniela Rus, Sangeeta N. Bhatia, and Connor W. Coley. Evidential deep learning for guided molecular property prediction and discovery. *ACS Central Science*, 7(8):1356–1367, 2021.
- [19] Jakob Gawlikowski, Sudipan Saha, Anna Kruspe, and Xiao Xiang Zhu. An advanced Dirichlet prior network for out-of-distribution detection in remote sensing. *IEEE Transactions on Geoscience and Remote Sensing*, 60:1–19, 2022.
- [20] Andrew Gelman, John B. Carlin, Hal S. Stern, David B. Dunson, Aki Vehtari, and Donald B. Rubin. *Bayesian Data Analysis*. Chapman and Hall/CRC, 3rd ed. edition, 2013.
- [21] Tianqi Chen and Carlos Guestrin. XGBoost: A scalable tree boosting system. In *Proceedings of the 22nd ACM SIGKDD International Conference on Knowledge Discovery and Data Mining, KDD '16*, page 785–794, 2016.
- [22] Guolin Ke, Qi Meng, Thomas Finley, Taifeng Wang, Wei Chen, Weidong Ma, Qiwei Ye, and Tie-Yan Liu. LightGBM: A highly efficient gradient boosting decision tree. In *Advances in Neural Information Processing Systems*, volume 30, 2017.
- [23] C’edric Villani. *Topics in Optimal Transportation*. American Mathematical Society, 2003.
- [24] Luigi Ambrosio, Nicola Gigli, and Giuseppe Savaré. *Gradient Flows In Metric Spaces and in the Space of Probability Measures*. Birkhäuser Basel, 2005.
- [25] Filippo Santambrogio. {Euclidean, metric, and Wasserstein} gradient flows: an overview. *Bulletin of Mathematical Sciences*, 7:87–154, 2017.
- [26] Qiang Liu. Stein variational gradient descent as gradient flow. In *Advances in Neural Information Processing Systems*, volume 30, 2017.
- [27] Jos’e Antonio Carrillo, Katy Craig, and Francesco S. Patacchini. A blob method for diffusion. *Calculus of Variations and Partial Differential Equations*, 58(53), 2019.

- [28] Yifei Wang, Peng Chen, and Wuchen Li. Projected Wasserstein gradient descent for high-dimensional Bayesian inference. *SIAM/ASA Journal on Uncertainty Quantification*, 10(4):1513–1532, 2022.
- [29] Dimitra Maoutsa, Sebastian Reich, and Manfred Opper. Interacting particle solutions of Fokker-Planck equations through gradient-log-density estimation. *Entropy (Basel)*, 22(8):802, 2020.
- [30] Ye He, Krishnakumar Balasubramanian, Bharath K. Sriperumbudur, and Jianfeng Lu. Regularized Stein variational gradient flow. *arXiv:2211.07861*, 2022.
- [31] Jerome H. Friedman. Greedy function approximation: A gradient boosting machine. *The Annals of Statistics*, 29(5):1189–1232, 2001.
- [32] Tony Duan, Avati Anand, Daisy Yi Ding, Khanh K. Thai, Sanjay Basu, Andrew Ng, and Alejandro Schuler. NGBoost: Natural gradient boosting for probabilistic prediction. In *Proceedings of the 37th International Conference on Machine Learning*, volume 119 of *Proceedings of Machine Learning Research*, pages 2690–2700. PMLR, 2020.
- [33] Peter Bühlmann and Torsten Hothorn. Boosting Algorithms: Regularization, Prediction and Model Fitting. *Statistical Science*, 22(4):477 – 505, 2007.
- [34] Leo Grinsztajn, Edouard Oyallon, and Gael Varoquaux. Why do tree-based models still outperform deep learning on typical tabular data? In *Advances in Neural Information Processing Systems*, volume 35, pages 507–520, 2022.
- [35] Piotr Florek and Adam Zagdański. Benchmarking state-of-the-art gradient boosting algorithms for classification. *arXiv:2305.17094*, 2023.
- [36] Zhendong Zhang and Cheolkon Jung. GBDT-MO: Gradient-boosted decision trees for multiple outputs. *IEEE Transactions on Neural Networks and Learning Systems*, 32(7):3156–3167, 2021.
- [37] Tianqi Chen, Sameer Singh, Ben Taskar, and Carlos Guestrin. Efficient Second-Order Gradient Boosting for Conditional Random Fields. In *Proceedings of the Eighteenth International Conference on Artificial Intelligence and Statistics*, volume 38 of *Proceedings of Machine Learning Research*, pages 147–155. PMLR, 2015.
- [38] Jerome H. Friedman. Stochastic gradient boosting. *Computational Statistics & Data Analysis*, 38(4):367–378, 2002.
- [39] Gianluca Detommaso, Tiangang Cui, Youssef Marzouk, Alessio Spantini, and Robert Scheichl. A Stein variational Newton method. In *Advances in Neural Information Processing Systems*, volume 31, 2018.
- [40] Yifei Wang and Wuchen Li. Information Newton’s flow: second-order optimization method in probability space. *arXiv:2001.04341*, 2020.
- [41] Malay Ghosh. Objective priors: An introduction for frequentists. *Statistical Science*, 26(2):187–202, 2011.
- [42] J. Aitchison and S. M. Shen. Logistic-normal distributions: Some properties and uses. *Biometrika*, 67(2):261–272, 1980.
- [43] Qiang Liu and Dilin Wang. Stein variational gradient descent: A general purpose Bayesian inference algorithm. In *Advances in Neural Information Processing Systems*, volume 29, 2016.
- [44] Dilin Wang, Zhe Zeng, and Qiang Liu. Stein variational message passing for continuous graphical models. In *Proceedings of the 35th International Conference on Machine Learning*, volume 80 of *Proceedings of Machine Learning Research*, pages 5219–5227. PMLR, 2018.
- [45] Alexander Lambert, Fabio Ramos, Byron Boots, Dieter Fox, and Adam Fishman. Stein variational model predictive control. In *Proceedings of the 2020 Conference on Robot Learning*, volume 155 of *Proceedings of Machine Learning Research*, pages 1278–1297. PMLR, 2021.

- [46] Anna Korba, Adil Salim, Michael Arbel, Giulia Luise, and Arthur Gretton. A non-asymptotic analysis for Stein variational gradient descent. In *Advances in Neural Information Processing Systems*, volume 33, pages 4672–4682, 2020.
- [47] Sinho Chewi, Thibaut Le Gouic, Chen Lu, Tyler Maunu, and Philippe Rigollet. SVGD as a kernelized Wasserstein gradient flow of the chi-squared divergence. In *Advances in Neural Information Processing Systems*, volume 33, pages 2098–2109, 2020.
- [48] Andre Wibisono. Sampling as optimization in the space of measures: The Langevin dynamics as a composite optimization problem. In *Proceedings of the 31st Conference On Learning Theory*, volume 75 of *Proceedings of Machine Learning Research*, pages 2093–3027. PMLR, 2018.
- [49] Gareth O. Roberts and Richard L. Tweedie. Exponential convergence of Langevin distributions and their discrete approximations. *Bernoulli*, 2(4):341 – 363, 1996.
- [50] Jose Miguel Hernandez-Lobato and Ryan Adams. Probabilistic backpropagation for scalable learning of Bayesian neural networks. In *Proceedings of the 32nd International Conference on Machine Learning*, volume 37 of *Proceedings of Machine Learning Research*, pages 1861–1869. PMLR, 2015.
- [51] Leo Breiman, Jerome Friedman, R.A. Olshen, and Charles J. Stone. *Classification and Regression Trees*. Chapman and Hall/CRC, 1984.
- [52] Trevor Hastie, Robert Tibshirani, and Jerome Friedman. *The Elements of Statistical Learning*. Springer New York, 2009.
- [53] Sanford Weisberg. *Applied Linear Regression*. John Wiley & Sons, 1985.
- [54] Dheeru Dua and Casey Graff. UCI machine learning repository, 2017.
- [55] Yarin Gal, Jiri Hron, and Alex Kendall. Concrete dropout. In *Advances in Neural Information Processing Systems*, volume 30, 2017.
- [56] Jingkang Yang, Kaiyang Zhou, Yixuan Li, and Ziwei Liu. Generalized out-of-distribution detection: A survey. *arXiv:2110.11334*, 2024.
- [57] Andrey Malinin, Bruno Mlodozieniec, and Mark Gales. Ensemble distribution distillation. In *International Conference on Learning Representations*, 2020.
- [58] Filippo Santambrogio. *Optimal Transport for Applied Mathematicians*. Birkhäuser Cham, 2015.
- [59] Mingxuan Yi and Song Liu. Bridging the gap between variational inference and Wasserstein gradient flows, 2023.
- [60] Michael Arbel, Anna Korba, Adil Salim, and Arthur Gretton. Maximum mean discrepancy gradient flow. In *Advances in Neural Information Processing Systems*, volume 32, 2019.
- [61] Richard Jordan, David Kinderlehrer, and Felix Otto. The variational formulation of the Fokker–Planck equation. *SIAM Journal on Mathematical Analysis*, 29(1):1–17, 1998.
- [62] Grigorios A. Pavliotis. *Stochastic Processes and Applications*. Springer New York, 2014.
- [63] Vern I. Paulsen and Mrinal Raghupathi. *An Introduction to the Theory of Reproducing Kernel Hilbert Spaces*. Cambridge University Press, 2016.
- [64] Alex Leviyev, Joshua Chen, Yifei Wang, Omar Ghattas, and Aaron Zimmerman. A stochastic Stein variational Newton method. *arXiv:2204.09039*, 2022.
- [65] Alex Smola, Arthur Gretton, Le Song, and Bernhard Schölkopf. A Hilbert space embedding for distributions.
- [66] Shun ichi Amari. *Information Geometry and Its Applications*. Springer Tokyo, 2016.

# Appendix

This appendix contains the technical and experiment details referred to in the main text. Appendix A recaps the derivation of the Wasserstein gradient and presents several examples. Appendix B discusses a variant of WGBost for the KL divergence built on the unadjusted Langevin algorithm. Appendix C derives the diagonal approximate Wasserstein Newton direction used for WEvidential. Appendix D provides a simulation study to compare four different WGBost algorithms. Appendix E describes the additional details of the experiment in the main text.

## A Derivation and Example of Wasserstein Gradient

This section recaps the derivation of the Wasserstein gradient of a functional  $\mathcal{F}$ , with examples of common divergences. The Wasserstein gradient depends on a function on  $\Theta$  called the *first variation* [24]. The first variation  $\delta\mathcal{F}(\mu)/\delta\mu$  of the functional  $\mathcal{F}$  at  $\mu$  is a function on  $\Theta$  that satisfies

$$\lim_{\epsilon \rightarrow 0^+} \frac{\mathcal{F}(\mu + \epsilon\nu) - \mathcal{F}(\mu)}{\epsilon} = \int_{\Theta} \frac{\delta\mathcal{F}(\mu)}{\delta\mu}(\theta)\nu(\theta)d\theta$$

for all signed measure  $\nu$  s.t.  $\mu + \epsilon\nu \in \mathcal{P}_2$  for all  $\epsilon$  sufficiently small. The Wasserstein gradient  $\nabla_W\mathcal{F}(\mu)$  of the functional  $\mathcal{F}$  at  $\mu$  is derived as the gradient of the first variation (see [e.g. 24]):

$$[\nabla_W\mathcal{F}(\mu)](\theta) := \nabla \frac{\delta\mathcal{F}(\mu)}{\delta\mu}(\theta).$$

It is common to suppose that the functional  $\mathcal{F}$  consists of three energies, which are determined by functions  $U : \mathbb{R} \rightarrow \mathbb{R}$ ,  $V : \Theta \rightarrow \mathbb{R}$ , and  $W : \Theta \times \Theta \rightarrow \mathbb{R}$  respectively, such that

$$\mathcal{F}(\mu) = \underbrace{\int_{\Theta} U(\mu(\theta))d\theta}_{\text{internal energy}} + \underbrace{\int_{\Theta} V(\theta)\mu(\theta)d\theta}_{\text{potential energy}} + \underbrace{\frac{1}{2} \int_{\Theta \times \Theta} W(\theta - \theta')\mu(\theta)d\theta\mu(\theta')d\theta'}_{\text{interaction energy}}.$$

For a functional  $\mathcal{F}$  that falls into the above form, the Wasserstein gradient is derived as

$$[\nabla_W\mathcal{F}(\mu)](\theta) = \nabla U'(\mu(\theta)) + \nabla V(\theta) + \int_{\Theta} \nabla W(\theta - \theta')\mu(\theta')d\theta'$$

where  $U'$  is the derivative of  $U : \mathbb{R} \rightarrow \mathbb{R}$  [23]. The KL divergence  $\mathcal{F}(\mu) = \text{KL}(\mu | \pi)$  of a distribution  $\mu$  falls into the form with  $U(x) = x \log x$ ,  $V(\theta) = -\log \pi(\theta)$ , and  $W(\theta) = 0$ , where

$$\text{KL}(\mu | \pi) = \int_{\Theta} \log \mu(\theta)\mu(\theta)d\theta + \int_{\Theta} -\log \pi(\theta)\mu(\theta)d\theta.$$

Table 3 presents examples of Wasserstein gradients of common divergences  $\mathcal{F}(\mu) = \text{D}(\mu | \pi)$ .

In the context of Bayesian inference, the KL divergence is particularly useful among many divergences. The Wasserstein gradient of the KL divergence requires no normalising constant of a posterior distribution  $\mu$ . This is because the Wasserstein gradient depends only on the log-gradient of the posterior  $\nabla \log \pi(\theta) = \nabla \pi(\theta)/\pi(\theta)$  of the target  $\pi$ , in which case the normalising constant of the target  $\pi$  is cancelled out by fraction. Hence, any posterior known only up to the normalising constant can be used as the target distribution  $\pi$  in the Wasserstein gradient of the KL divergence.



Table 3: Wasserstein gradients of four divergences: the KL divergence [58], the chi-squared divergence [47], the alpha divergence [59], and the maximum mean discrepancy [60].

Divergence $\mathcal{F}(\mu) = D(\mu   \pi)$	Wasserstein gradient $[\nabla_W \mathcal{F}(\mu)](\theta)$
KL( $\mu   \pi$ )	$-(\nabla \log \pi(\theta) - \nabla \log \mu(\theta))$
Chi <sup>2</sup> ( $\mu   \pi$ )	$2\nabla(\mu(\theta)/\pi(\theta))$
Alpha( $\mu   \pi$ )	$(\mu(\theta)/\pi(\theta))^{\alpha-1} \nabla(\mu(\theta)/\pi(\theta))$
MMD( $\mu   \pi$ )	$\int_{\Theta} \nabla k(\theta, \theta') \mu(\theta) d\theta - \int_{\Theta} \nabla k(\theta, \theta') \pi(\theta) d\theta$

## B Langevin Gradient Boosting for KL Divergence

If a chosen functional  $\mathcal{F}$  on  $\mathcal{P}_2$  is the KL divergence  $\mathcal{F}(\mu) = \text{KL}(\mu | \pi)$  of a target distribution  $\pi$ , the continuity equation (1) admits an equivalent representation as the Fokker-Planck equation [61]:

$$\frac{d}{dt} \mu_t = \nabla \cdot (\mu_t \nabla \log \pi) + \Delta \mu_t \quad \text{given } \mu_0 \in \mathcal{P}_2 \quad (10)$$

where  $\Delta$  denotes the Laplacian operator. Recall that the original continuity equation (1) can be reformulated as the deterministic differential equation (2) of a random variable  $\theta_t \sim \mu_t$ . In contrast, the Fokker-Planck equation (10) can be reformulated as a stochastic differential equation of a random variable  $\theta_t \sim \mu_t$ , known as the overdamped Langevin dynamics [62]:

$$d\theta_t = \nabla \log \pi(\theta_t) dt + \sqrt{2} dB_t \quad \text{given } \theta_0 \sim \mu_0, \quad (11)$$

where  $B_t$  denotes a standard Brownian motion. Note that the deterministic system (2) in the case of the KL divergence and the above stochastic system (11) are equivalent at population level, in a sense that the law of the random variable  $\theta_t$  in both the systems solves the two equivalent equations.

At the algorithmic level, however, discretisation of each system leads to different particle update schemes. Set the initial distribution  $\mu_0$  in (11) to the empirical distribution  $\hat{\mu}_0$  of  $N$  initial particles  $\{\theta_0^n\}_{n=1}^N$ . Discretising the stochastic system (11) by the Euler-Maruyama method with a step size  $\nu > 0$  yields a stochastic update scheme of particles  $\{\theta_m^n\}_{n=1}^N$  from step  $m = 0$ :

$$\begin{bmatrix} \theta_{m+1}^1 \\ \vdots \\ \theta_{m+1}^N \end{bmatrix} = \begin{bmatrix} \theta_m^1 \\ \vdots \\ \theta_m^N \end{bmatrix} + \nu \begin{bmatrix} \nabla \log \pi(\theta_m^1) + \sqrt{2/\nu} \xi^1 \\ \vdots \\ \nabla \log \pi(\theta_m^N) + \sqrt{2/\nu} \xi^N \end{bmatrix},$$

where each  $\xi^n$  denotes a realisation from a standard normal distribution on  $\mathbb{R}^d$ . The above updating scheme of each  $n$ -th particle is known as the unadjusted Langevin algorithm [49]. We can define a variant of WGBost by replacing the term  $\mathcal{G}_i(\mu)$  in Algorithm 1 with  $\nabla \log \mu_i(\cdot) + \sqrt{2/\nu} \xi_i$  where  $\mu_i$  is an output distribution at each  $x_i$  and  $\xi_i$  is a realisation from a standard normal distribution. The procedure is summarised in Algorithm 3, which we call Langevin gradient boosting (LGBoost).

## C Derivation of Approximate Wasserstein Newton Direction

This section derives the diagonal approximate Wasserstein Newton direction based on the kernel smoothing. The approximate Wasserstein Newton direction of the KL divergence was derived in [39] under a different terminology—simply, the Newton direction—from a viewpoint of nonparametric variational inference. We place their result in the context of approximate Wasserstein gradient flows. Appendix C.1 shows the derivation of the smoothed Wasserstein gradient and Hessian. Appendix C.2 defines the Newton direction built upon the smoothed Wasserstein gradient and Hessian, following the derivation in [39]. Appendix C.3 derives the diagonal approximation of the Newton direction.

---

**Algorithm 3: Langevin Gradient Boosting**

---

**Input:** training set  $\{x_i, \mu_i\}_{i=1}^D$  of input  $x_i \in \mathcal{X}$  and output distribution  $\mu_i \in \mathcal{P}_2$

**Parameter:** particle number  $N$ , iteration  $M$ , rate  $\nu$ , weak learner  $f$ , initial constants  $(\vartheta_0^1, \dots, \vartheta_0^N)$

**Output:** set of  $N$  boosting ensembles  $(F_M^1, \dots, F_M^N)$  at final step  $M$

$(F_0^1(\cdot), \dots, F_0^N(\cdot)) \leftarrow (\vartheta_0^1, \dots, \vartheta_0^N)$

**for**  $m \leftarrow 0, \dots, M-1$  **do**

**for**  $n \leftarrow 1, \dots, N$  **do**

**for**  $i \leftarrow 1, \dots, D$  **do**

$g_i^n \leftarrow \nabla \log \mu_i(F_m^n(x_i)) + \sqrt{2/\nu} \xi_i^n$  where  $\xi_i^n \sim \mathcal{N}(0, I_d)$

**end**

$f_{m+1}^n \leftarrow \text{fit}(\{x_i, g_i^n\}_{i=1}^D)$

$F_{m+1}^n(\cdot) \leftarrow F_m^n(\cdot) + \nu f_{m+1}^n(\cdot)$

**end**

**end**

---

### C.1 Smoothed Wasserstein Gradient and Hessian

Consider the one-dimensional case  $\Theta = \mathbb{R}$  for simplicity. For a map  $T : \mathbb{R} \rightarrow \mathbb{R}$  and a distribution  $\mu \in \mathcal{P}_2$ , let  $\mu_t$  be the pushforward of  $\mu$  under the transform  $\theta \mapsto \theta + tT(\theta)$  defined with a time-variable  $t \in \mathbb{R}$ . This means that  $\mu_t$  is a distribution obtained by change-of-variable applied for  $\mu$ . The Wasserstein gradient of a functional  $\mathcal{F}(\mu)$  can be associated with the time derivative  $(d/dt)\mathcal{F}(\mu_t)$  [23]. In what follows, we focus on the KL divergence  $\mathcal{F}(\mu) = \text{KL}(\mu | \pi)$  as a loss functional. Under a condition  $T \in L^2(\mu)$ , the time derivative at  $t = 0$  satisfies the following equality

$$\left. \frac{d}{dt} \text{KL}(\mu_t | \pi) \right|_{t=0} = \int_{\Theta} T(\theta) [\mathcal{G}^{\text{KL}}(\mu)](\theta) d\mu(\theta) = \langle T, \mathcal{G}^{\text{KL}}(\mu) \rangle_{L^2(\mu)}, \quad (12)$$

where  $\mathcal{G}^{\text{KL}}(\mu)$  denotes the Wasserstein gradient of  $\mathcal{F}(\mu) = \text{KL}(\mu | \pi)$  with the target distribution  $\pi$  made implicit. It gives an interpretation of the Wasserstein gradient as the steepest-descent direction because the decay of the KL divergence at  $t = 0$  is maximised when  $T = -\mathcal{G}^{\text{KL}}(\mu)$ .

The ‘smoothed’ Wasserstein gradient can be derived by restricting the transform map  $T$  to a more regulated Hilbert space than  $L^2(\mu)$ . A reproducing kernel Hilbert space (RKHS)  $H$  associated with a kernel function  $k : \mathbb{R} \times \mathbb{R} \rightarrow \mathbb{R}$  is the most common choice of such a Hilbert space [e.g. 26]. An important property of the RKHS  $H$  is that any function  $f \in H$  satisfies the *reproducing property*  $f(\theta) = \langle f(\cdot), k(\cdot, \theta) \rangle_H$  under the associated kernel  $k$  and inner product  $\langle \cdot, \cdot \rangle_H$  [63]. As discussed in [e.g. 46], applying the reproducing property in (12) under the condition  $T \in H$  and exchanging the integral order, the time derivative satisfies an alternative equality as follows:

$$\begin{aligned} \left. \frac{d}{dt} \text{KL}(\mu_t | \pi) \right|_{t=0} &= \int_{\Theta} \langle T(\cdot), k(\cdot, \theta) \rangle_H [\mathcal{G}^{\text{KL}}(\mu)](\theta) d\mu(\theta) \\ &= \left\langle T(\cdot), \int_{\Theta} [\mathcal{G}^{\text{KL}}(\mu)](\theta) k(\cdot, \theta) d\mu(\theta) \right\rangle_H = \langle T, \mathcal{G}^*(\mu) \rangle_H \end{aligned} \quad (13)$$

where  $[\mathcal{G}^*(\mu)](\cdot) := \int_{\Theta} [\mathcal{G}^{\text{KL}}(\mu)](\theta) k(\cdot, \theta) d\mu(\theta)$  corresponds to the smoothed Wasserstein gradient used in the main text. The decay of the KL divergence at  $t = 0$  is maximised by  $T = -\mathcal{G}^*(\mu)$ .

Similarly, the Wasserstein Hessian of the functional  $\mathcal{F}(\mu)$  can be associated with the second time derivative  $(d^2/dt^2)\mathcal{F}(\mu_t)$  [23]. As discussed in [e.g. 46], the Wasserstein Hessian of the KL divergence, denoted  $\text{Hess}(\mu)$ , is an operator over functions  $T \in L^2(\mu)$  that satisfies

$$\left. \frac{d^2}{dt^2} \text{KL}(\mu_t | \pi) \right|_{t=0} = \langle T, \text{Hess}(\mu)T \rangle_{L^2(\mu)}. \quad (14)$$

See [46] for the explicit form of the Wasserstein Hessian. In the same manner as the smoothed Wasserstein gradient, applying the reproducing property in (14) under the condition  $T \in H$  and exchanging the integral order, the second time derivative satisfies an alternative equality as follows:

$$\frac{d^2}{dt^2} \text{KL}(\mu_t | \pi) \Big|_{t=0} = \left\langle T(\star_1), \left\langle [\text{Hess}^*(\mu)](\star_1, \star_2), T(\star_2) \right\rangle_H \right\rangle_H \quad (15)$$

where  $[\text{Hess}^*(\mu)](\star_1, \star_2) := \langle k(\star_1, \cdot), \text{Hess}(\mu)k(\star_2, \cdot) \rangle_{L^2(\mu)}$  is the smoothed Wasserstein Hessian and the symbols  $\star_1$  and  $\star_2$  denote the variables to which each of the two inner products is taken.

In the multidimensional case  $\Theta = \mathbb{R}^d$ , the transport map  $T$  is a vector-valued function  $T : \mathbb{R}^d \rightarrow \mathbb{R}^d$ , where a similar derivation can be repeated by replacing  $L^2(\mu)$  and  $H$  with the product space of  $d$  independent copies of  $L^2(\mu)$  and  $H$ . It follows from Proposition 1 and Theorem 1 in [39]—which derives the explicit form of (13) and (15) under their terminology, first and second variations—that the explicit form of the smoothed Wasserstein gradient and Hessian is given by

$$\begin{aligned} [\mathcal{G}^*(\mu)](\cdot) &= \mathbb{E}_{\theta \sim \mu} \left[ -\nabla \log \pi(\theta) k(\cdot, \theta) - \nabla k(\cdot, \theta) \right] \in \mathbb{R}^d, \\ [\text{Hess}^*(\mu)](\star_1, \star_2) &= \mathbb{E}_{\theta \sim \mu} \left[ -\nabla^2 \log \pi(\theta) k(\star_1, \theta) k(\star_2, \theta) + \nabla k(\star_1, \theta) \otimes \nabla k(\star_2, \theta) \right] \in \mathbb{R}^{d \times d} \end{aligned}$$

where  $\nabla^2$  denotes an operator to take the Jacobian of the gradient—i.e.,  $\nabla^2 f(\theta)$  is the Hessian matrix of  $f$  at  $\theta$ —and  $\otimes$  denotes the outer product of two vectors. Note that both the smoothed Wasserstein gradient and Hessian are well-defined for any distribution  $\mu$  including empirical distributions.

## C.2 Approximate Wasserstein Newton Direction

In the Euclidean space, the Newton direction of an objective function is a direction s.t. the second-order Taylor approximation of the function is minimised. Similarly, [39] characterised the Newton direction  $T^* : \mathbb{R}^d \rightarrow \mathbb{R}^d$  of the KL divergence  $\text{KL}(\mu | \pi)$  as a solution of the following equation

$$\left\langle \left\langle [\text{Hess}^*(\mu)](\star_1, \star_2), T^*(\star_2) \right\rangle_H + [\mathcal{G}^*(\mu)](\star_1), V(\star_1) \right\rangle_H = 0 \quad \text{for all } V \in H.$$

Here  $\Theta = \mathbb{R}^d$  and  $H$  is the product space of  $d$  independent copies of the RKHS of a kernel  $k$ . To obtain a closed-form solution, [39] supposed that the Newton direction  $T^*$  can be expressed in a form  $T^*(\cdot) = \sum_{i=1}^n W^i k(\cdot, \theta^i)$  dependent on a set of each particle  $\theta^i \in \Theta$  and associated vector-valued coefficient  $W^i \in \mathbb{R}^d$ . Once the set of the particles is given, the set of the associated vector-valued coefficients is determined by solving the following simultaneous linear equation

$$\begin{bmatrix} \sum_{n=1}^N [\text{Hess}^*(\mu)](\theta^1, \theta^n) \cdot W^n \\ \vdots \\ \sum_{n=1}^N [\text{Hess}^*(\mu)](\theta^N, \theta^n) \cdot W^n \end{bmatrix} = \begin{bmatrix} -[\mathcal{G}^*(\mu)](\theta^1) \\ \vdots \\ -[\mathcal{G}^*(\mu)](\theta^N) \end{bmatrix}. \quad (16)$$

These equations (16) can be rewritten in a matrix form [64]. Let  $K := N \times d$ . Define a block matrix  $\mathbf{H} \in \mathbb{R}^{K \times K}$  and a block vector  $\mathbf{G} \in \mathbb{R}^K$  by the following partitioning

$$\mathbf{H} = \left( \begin{array}{c|c|c} \mathbf{H}_{11} & \cdots & \mathbf{H}_{1N} \\ \vdots & \ddots & \vdots \\ \mathbf{H}_{N1} & \cdots & \mathbf{H}_{NN} \end{array} \right) \quad \text{and} \quad \mathbf{G} = \left( \begin{array}{c} \mathbf{G}_1 \\ \vdots \\ \mathbf{G}_N \end{array} \right)$$

with each block specified as  $\mathbf{H}_{ij} := [\text{Hess}^*(\mu)](\theta^i, \theta^j) \in \mathbb{R}^{d \times d}$  and  $\mathbf{G}_i := [\mathcal{G}^*(\mu)](\theta^i) \in \mathbb{R}^d$ . Define a block matrix  $\mathbf{K} \in \mathbb{R}^{K \times K}$  and a block vector  $\mathbf{W} \in \mathbb{R}^K$  by the following partitioning

$$\mathbf{K} := \left( \begin{array}{c|c|c} \mathbf{K}_{11} & \cdots & \mathbf{K}_{1N} \\ \vdots & \ddots & \vdots \\ \mathbf{K}_{N1} & \cdots & \mathbf{K}_{NN} \end{array} \right) \quad \text{and} \quad \mathbf{W} := \left( \begin{array}{c} W^1 \\ \vdots \\ W^N \end{array} \right)$$

with each block of  $\mathbf{K}$  specified as  $\mathbf{K}_{ij} := \mathbf{I}_d \times k(\theta^i, \theta^j) \in \mathbb{R}^{d \times d}$ , where  $\mathbf{I}_d$  denotes the  $d \times d$  identity matrix. Notice that  $\mathbf{W}$  is a block vector that aligns the vector-valued coefficients  $\{W^n\}_{n=1}^N$ . Using these notations, the optimal coefficients that solve (16) is simply written as  $\mathbf{W} = -\mathbf{H}^{-1}\mathbf{G}$  [64].

Given the optimal coefficients  $\mathbf{W} = -\mathbf{H}^{-1}\mathbf{G}$ , the Newton direction  $T^*(\theta^n)$  evaluated at the given particle  $\theta^n$  for each  $n = 1, \dots, N$  can be written in the following block vector form

$$\begin{pmatrix} T^*(\theta^1) \\ \vdots \\ T^*(\theta^N) \end{pmatrix} = - \begin{pmatrix} \mathbf{K}_{11} & \cdots & \mathbf{K}_{1N} \\ \vdots & \ddots & \vdots \\ \mathbf{K}_{N1} & \cdots & \mathbf{K}_{NN} \end{pmatrix} \begin{pmatrix} \mathbf{H}_{11} & \cdots & \mathbf{H}_{1N} \\ \vdots & \ddots & \vdots \\ \mathbf{H}_{N1} & \cdots & \mathbf{H}_{NN} \end{pmatrix}^{-1} \begin{pmatrix} \mathbf{G}_1 \\ \vdots \\ \mathbf{G}_N \end{pmatrix} \quad (17)$$

To distinguish from the standard Newton direction in the Euclidean space, we call (17) the approximate Wasserstein Newton direction. The approximate Wasserstein Newton direction yields a second-order particle update scheme. Suppose we have particles  $\{\theta_m^n\}_{n=1}^N$  to be updated at each step  $m$ . At each step  $m$ , define the above matrices  $\mathbf{H}$  and  $\mathbf{G}$  with the empirical distribution  $\mu = \hat{\pi}_m$  of the particles  $\{\theta_m^n\}_{n=1}^N$ . Replacing the Wasserstein gradient in the particle update scheme (3) by the approximate Wasserstein Newton direction (17) provides the second-order update scheme in [39].

### C.3 Diagonal Approximate Wasserstein Newton Direction

We derive the diagonal approximation of the approximate Wasserstein Newton direction, which we used for our second-order WGBost algorithm. A few approximations of the approximate Wasserstein Newton direction were discussed in [39] for better performance of their particle algorithm. We derive the diagonal approximation so that no matrix product and inversion will be involved. Specifically, we replace the matrices  $\mathbf{K}$  and  $\mathbf{H}$  in (17) by the diagonal approximations  $\hat{\mathbf{K}}$  and  $\hat{\mathbf{H}}$ , that is,

$$\hat{\mathbf{K}} = \begin{pmatrix} \mathbf{I}_d & \cdots & \mathbf{0} \\ \vdots & \ddots & \vdots \\ \mathbf{0} & \cdots & \mathbf{I}_d \end{pmatrix} \quad \text{and} \quad \hat{\mathbf{H}} = \begin{pmatrix} \mathbf{h}_{11} & \cdots & \mathbf{0} \\ \vdots & \ddots & \vdots \\ \mathbf{0} & \cdots & \mathbf{h}_{NN} \end{pmatrix},$$

where  $\mathbf{K}_{nn} = \mathbf{I}_d \times k(\theta^n, \theta^n) = \mathbf{I}_d$  for the Gaussian kernel  $k$  used in this work, and the matrix  $\mathbf{h}_{nn} \in \mathbb{R}^{d \times d}$  denotes the diagonal approximation of the diagonal block  $\mathbf{H}_{nn}$  of  $\mathbf{H}$ .

Recall that  $\mathbf{H}_{nn} = [\text{Hess}^*(\mu)](\theta^n, \theta^n)$ . Denote by  $\text{Diag}(\mathbf{A})$  the diagonal of a square matrix  $\mathbf{A}$ . The diagonal approximation  $\mathbf{h}_{nn}$  is a diagonal matrix whose diagonal is  $\text{Diag}(\mathbf{H}_{nn})$ . We plug the diagonal approximations  $\hat{\mathbf{K}}$  and  $\hat{\mathbf{H}}$  in (17). It follows from inverse and multiplication properties of diagonal matrices that the approximate Wasserstein Newton direction turns into a form

$$\begin{pmatrix} T^*(\theta^1) \\ \vdots \\ T^*(\theta^N) \end{pmatrix} = - \begin{pmatrix} \mathbf{h}_{11} & \cdots & \mathbf{0} \\ \vdots & \ddots & \vdots \\ \mathbf{0} & \cdots & \mathbf{h}_{NN} \end{pmatrix}^{-1} \begin{pmatrix} \mathbf{G}_1 \\ \vdots \\ \mathbf{G}_N \end{pmatrix} = \begin{pmatrix} -\mathbf{G}_1 \oslash \text{Diag}(\mathbf{H}_{11}) \\ \vdots \\ -\mathbf{G}_N \oslash \text{Diag}(\mathbf{H}_{NN}) \end{pmatrix}. \quad (18)$$

At an arbitrary particle location  $\theta$ , denote by  $[\mathcal{H}^*(\mu)](\theta)$  the diagonal of the smoothed Wasserstein Hessian  $[\text{Hess}^*(\mu)](\theta, \theta)$ . It is straightforward to see that the diagonal can be written as

$$[\mathcal{H}^*(\mu)](\cdot) = \mathbb{E}_{\theta \sim \mu} \left[ -\nabla_d^2 \log \pi(\theta) k(\cdot, \theta)^2 + \nabla k(\cdot, \theta) \odot \nabla k(\cdot, \theta) \right].$$

Notice that  $\text{Diag}(\mathbf{H}_{nn}) = [\mathcal{H}^*(\mu)](\theta^n)$  by definition. It therefore follows from the formula (18) with  $\mathbf{G}_n = [\mathcal{G}^*(\mu)](\theta^n)$  and  $\text{Diag}(\mathbf{H}_{nn}) = [\mathcal{H}^*(\mu)](\theta^n)$  that the diagonal approximate Wasserstein Newton direction at an arbitrary particle location  $\theta$  can be independently computed by

$$-[\mathcal{G}^*(\mu)](\theta) \oslash [\mathcal{H}^*(\mu)](\theta).$$

We used this direction in Section 3. In the main text, the diagonal approximate Wasserstein Newton direction is defined for each loss functional  $\mathcal{F}_i(\cdot) = \text{D}(\cdot \mid \mu_i)$ , with  $\pi = \mu_i$ , using the smoothed Wasserstein gradient  $\mathcal{G}_i^*(\mu)$  and the diagonal of the smoothed Wasserstein Hessian  $\mathcal{H}_i^*(\mu)$  for each  $i$ -th output distribution  $\mu_i$ .

## D Comparison of Different WBoost Algorithms

We compare four different algorithms of WBoost for the KL divergence through a simulation study. The first three algorithms are defined by setting the term  $\mathcal{G}_i(\mu)$  in Algorithm 1 to, respectively,

1. the smoothed Wasserstein gradient in (7);
2. the diagonal approximate Wasserstein Newton direction in (8);
3. the full approximate Wasserstein Newton direction in (17).

The fourth algorithm, which is rather a variant of WBoost, is LBoost in Appendix B. The first and third WBoost algorithms is called, respectively, first-order WEvidential and full-Newton WEvidential. The second WBoost algorithm is WEvidential presented in Section 3. We fit the four algorithms to a synthetic dataset  $\{x_i, \mu_i\}_{i=1}^D$  whose inputs are 200 grid points on the interval  $[-3.5, 3.5]$  and output distributions are normal distributions  $\mu_i(\theta) = \mathcal{N}(\theta \mid \sin(x_i), 0.5)$  conditional on each  $x_i$ .

The first-order WEvidential is implemented by Algorithm 2 removing  $h_i^n$  and replacing  $g_i^n \circ h_i^n$  with  $g_i^n$ . The full-Newton WEvidential is implemented by Algorithm 2 replacing  $g_i^n \circ h_i^n$  with  $v_i^n$  computed by the following Algorithm 4, where  $\nabla^2 f(\theta)$  denotes the Hessian matrix of a function  $f : \Theta \rightarrow \mathbb{R}$  at  $\theta$ .

---

### Algorithm 4: Computation of Approximate Wasserstein Newton Direction

---

**Input:** input  $x_i$ , output distribution  $\mu_i$ , outputs of  $N$  boostings  $(F_m^1(x_i), \dots, F_m^N(x_i))$  for input  $x_i$

**Output:** Wasserstein Newton direction  $(v_i^1, \dots, v_i^N)$  evaluated at  $(F_m^1(x_i), \dots, F_m^N(x_i))$  for input  $x_i$

$\hat{\mu}_{m,i} \leftarrow$  empirical distribution of set of  $N$  outputs  $(F_m^1(x_i), \dots, F_m^N(x_i))$  for input  $x_i$

**for**  $n \leftarrow 1, \dots, N$  **do**

$g_i^n \leftarrow \mathbb{E}_{\theta^* \sim \hat{\mu}_{m,i}} [\nabla \log \mu(\theta^*) k(F_m^n(x_i), \theta^*) + \nabla k(F_m^n(x_i), \theta^*)]$

**for**  $k \leftarrow 1, \dots, N$  **do**

$H_i^{nk} \leftarrow \mathbb{E}_{\theta^* \sim \hat{\mu}_{m,i}} [-\nabla^2 \log \mu_i(\theta^*) k(F_m^n(x_i), \theta^*) k(F_m^k(x_i), \theta^*) + \nabla k(F_m^n(x_i), \theta^*) \otimes \nabla k(F_m^k(x_i), \theta^*)]$

$K_i^{nk} \leftarrow \mathbf{I}_d \cdot k(F_m^n(x_i), F_m^k(x_i))$

**end**

**end**

$$\begin{pmatrix} v_i^1 \\ \vdots \\ v_i^N \end{pmatrix} \leftarrow \begin{pmatrix} K_i^{11} & \dots & K_i^{1N} \\ \vdots & \ddots & \vdots \\ K_i^{N1} & \dots & K_i^{NN} \end{pmatrix}^{-1} \begin{pmatrix} H_i^{11} & \dots & H_i^{1N} \\ \vdots & \ddots & \vdots \\ H_i^{N1} & \dots & H_i^{NN} \end{pmatrix} \begin{pmatrix} g_i^1 \\ \vdots \\ g_i^N \end{pmatrix}$$


---

Figure 5 shows the performance and computational time of each algorithm on the synthetic data with respect to the number of weak learners. We computed the output of each algorithm for 500 grid points in the interval  $[-3.5, 3.5]$ . We used the maximum mean discrepancy (MMD) [65] to measure the approximation error between the empirical distribution  $\hat{\mu}_i$  of the output particles and the output distribution  $\mu_i$  at each input  $x_i$ :

$$\text{MMD}^2(\hat{\mu}_i, \mu_i) = \mathbb{E}_{\theta \sim \hat{\mu}_i, \theta' \sim \hat{\mu}_i} [k(\theta, \theta')] - 2\mathbb{E}_{\theta \sim \hat{\mu}_i, \theta' \sim \mu_i} [k(\theta, \theta')] + \mathbb{E}_{\theta \sim \mu_i, \theta' \sim \mu_i} [k(\theta, \theta')]$$

where  $k$  is a Gaussian kernel  $k(\theta, \theta') = \exp(-(\theta - \theta')^2/h)$  with scale hyperparameter  $h = 0.025$ . The total approximation error was measured by the MMD averaged over all the inputs. We set the initial constant  $\{\vartheta^n\}_{n=1}^{10}$  of each algorithm to 10 grid points in the interval  $[-10, 10]$ , which sufficiently differs from the output distributions to observe the decay of the approximation error. The decision tree regressor with maximum depth 3 was used as weak learners for all the algorithm.

Figure 5 demonstrates that WEvidential and full-Newton WEvidential reduce the approximation error most efficiently, while full-Newton WEvidential takes the longest computational time among others. As in Algorithm 4, the computation of the full approximate Wasserstein Newton direction requires the inverse and

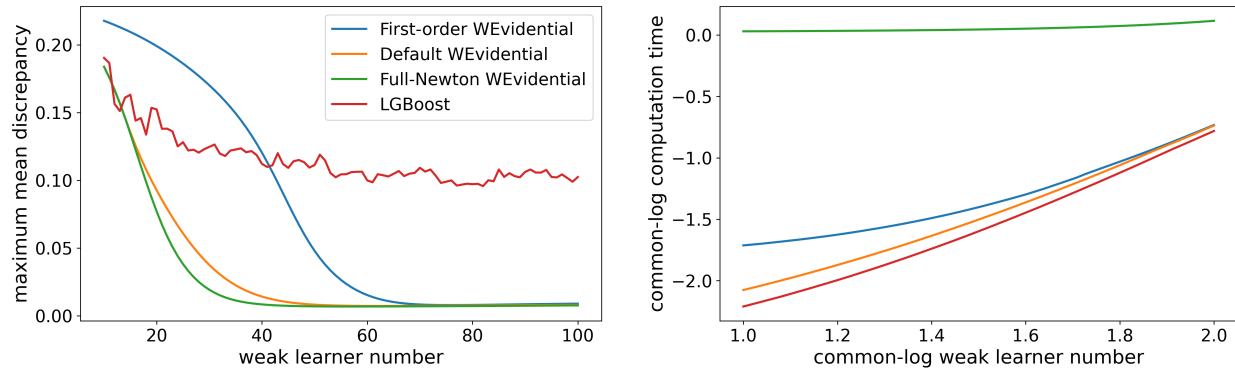


Figure 5: The approximation error and computational time of the four algorithms. Left: approximation error of each algorithm measured by the MMD averaged over the inputs. Right: computational time with respect to the weak learner number in common logarithm scale.

product of the  $(N \times d) \times (N \times d)$  block matrices, where  $N$  denotes the particle number  $N$  and  $d$  denotes the particle dimension. The computation of the diagonal approximate Wasserstein Newton direction requires only elementwise division of the  $d$ -dimensional vectors. The error decay of LGBoost is not as fast as the other WGBost algorithms, and also shows stochasticity due to the Gaussian noise used in the algorithm. We therefore recommend to use WEvidential for better performance and efficient computation. Figure 6 depicts the output of each algorithm with 100 weak learners trained.

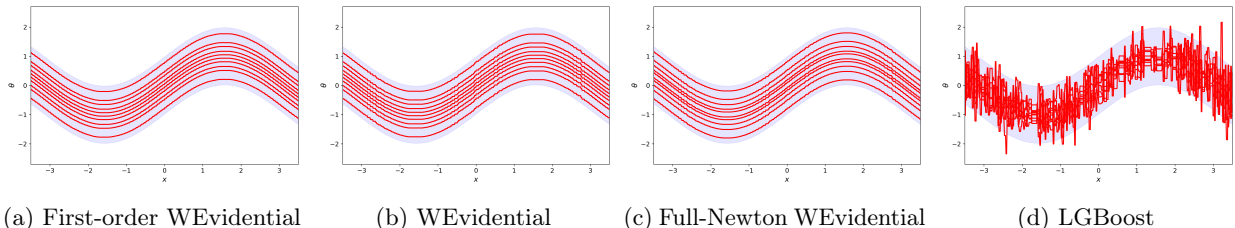


Figure 6: Illustration of the output of the four algorithms (red line) with 100 weak learners trained. The blue area corresponds to the 95% high probability region of each output distribution.

## E Additional Detail of Application

This section describes additional details of the applications in Section 4. All the experiments were performed with x86-64 CPUs, where some of them were parallelised up to 10 CPUs and the rest uses 1 CPU. The scripts to reproduce all the experiments are provided in the source code. Appendices E.1 to E.3 describe additional details of the applications in, respectively, Sections 4.1 to 4.3. Appendix E.4 describes a choice of initial constants  $\{\vartheta_0^n\}_{n=1}^N$  for the WGBost algorithm used in Section 4.

### E.1 Detail of Section 4.1

The normal response distribution  $\mathcal{N}(y | m, \sigma)$  in Example 1 was used in Section 4.1. The normal output distribution has the scale parameter  $\sigma$  that lies only in the positive domain of the Euclidean space  $\mathbb{R}$ . We reparametrised it as one in the Euclidean space  $\mathbb{R}$  by the log transform  $\sigma' := \log(\sigma)$ , which is the standard practice in Bayesian computation [20]. The inverse of the log transform is the exponential transform  $\sigma = \exp(\sigma')$ . It follows from change of variable that the individual-level posterior on  $(m, \sigma')$  conditional on

each individual observed response  $y_i$ , with the prior in Example 1, is given by

$$\mu_i(m, \sigma') = p(m, \sigma' | y_i) \propto \exp\left(-\frac{1}{2} \frac{(y_i - m)^2}{\exp(\sigma')^2}\right) \times \exp\left(-\frac{1}{2} \frac{m^2}{10^2}\right) \times \frac{1}{\exp(\sigma')^{1.01}} \exp\left(-\frac{0.01}{\exp(\sigma')}\right)$$

up to the normalising constant, where we used the Jacobian determinant  $|d\sigma/d\sigma'| = \exp(\sigma')$ .

## E.2 Detail of Section 4.2

The same reparametrisation of the normal output distribution as Appendix E.2 was used in Section 4.2. For test data  $\{x_i, y_i\}_{i=1}^D$ , the NLL and RMSE of each algorithm were computed by

$$\text{NLL} = -\frac{1}{D} \sum_{i=1}^D \log p(y_i | x_i) \quad \text{and} \quad \text{RMSE} = \sqrt{\frac{1}{D} \sum_{i=1}^D (y_i - \hat{y}_i)^2}$$

for the obtained provided predictive distribution  $p(y_i | x_i)$  and the point prediction  $\hat{y}_i$ . For WEvidential, the observed responses in training data were standardised. Accordingly, the test responses were standardised as  $y'_i = (y_i - y_{\text{mean}}^{\text{train}})/y_{\text{std}}^{\text{train}}$  using the mean  $y_{\text{mean}}^{\text{train}}$  and standard deviation  $y_{\text{std}}^{\text{train}}$  of the training responses. The predictive distribution  $p(y'_i | x_i)$  and point prediction  $\hat{y}'_i$  of WEvidential were provided for the standardised responses  $y'_i$ . The NLL and RMSE for the original responses  $y_i$  can be computed as follows:

$$\begin{aligned} \text{NLL} &= -\frac{1}{D} \sum_{i=1}^D \log p(y_i | x_i) = -\frac{1}{D} \sum_{i=1}^D \log p(y'_i | x_i) + \log y_{\text{std}}^{\text{train}}, \\ \text{RMSE} &= \sqrt{\frac{1}{D} \sum_{i=1}^D (y_i - (y_{\text{mean}}^{\text{train}} + y_{\text{std}}^{\text{train}} \times \hat{y}'_i))^2} = y_{\text{std}}^{\text{train}} \sqrt{\frac{1}{D} \sum_{i=1}^D (y'_i - \hat{y}'_i)^2} \end{aligned}$$

where the equality of the NLL follows from change of variable  $p(y_i | x_i) = p(y'_i | x_i)/y_{\text{std}}^{\text{train}}$  and the equality of the RMSE follows from rearranging the terms.

We provide a brief description of each algorithm used for the comparison. For each algorithm, the normal response distribution  $p(y | m, \sigma)$  was specified for the response variable and the algorithm produces a point or distributional estimate of the response parameter  $(m, \sigma)$  at each input  $x$ .

- MCDropout [9] trains a single neural network  $F$  while dropping out each network weight with some Bernoulli probability. It can be interpreted as a variational approximation of a Bayesian neural network. It generates multiple subnetworks  $\{F^n\}_{n=1}^N$  by subsampling the network weights by the dropout. The predictive distribution  $p(y | x)$  is given by the model averaging  $(1/N) \sum_{i=1}^N p(y | (m, \sigma) = F^n(x))$  for each input  $x$ .
- DEnsemble [10] simply trains independent copies  $\{F^n\}_{n=1}^N$  of a neural network  $F$  in parallel. It is one of the mainstream approaches to uncertainty quantification based on deep learning. The predictive distribution is given by the model averaging as in MCDropout.
- CDropout [55] consider a continuous relaxation of the Bernoulli random variable used in MCDropout to optimise the Bernoulli probability of the dropout. It generates multiple subnetworks  $\{F^n\}_{n=1}^N$  by subsampling the network weights by the dropout with the optimised probability. The predictive distribution is the same as MCDropout.
- NGBoosting [32] is a family of gradient booting that use the natural gradient [66] of the response distribution as a target variable of each weak learner. In contrast to other methods, NGBoost outputs a single value  $F(x)$  to be plugged into the response-distribution parameter. The predictive distribution  $p(y | x)$  is given by  $p(y | (m, \sigma) = F(x))$  for each input  $x$ .

- DEvidential [13] extends deep evidential learning [11], originally proposed in classification settings, to regression settings. It considers the case where the individual-level posterior of the response distribution falls into a conjugate parametric form, and predicts the hyperparameter of the individual-level posterior by a neural network. The predictive distribution is also given in a conjugate closed-form.

### E.3 Detail of Section 4.3

Similarly to the normal response distribution used in Sections 4.1 and 4.2, we reparametrised the parameter of the categorical response distribution used in Section 4.3. The categorical response distribution  $\mathcal{C}(y | q)$  in Example 2 has a class probability parameter  $q = [q_1, \dots, q_k]$  in the simplex  $\Delta_k$ . We reparametrised the parameter  $q$  by the log-ratio transform  $q' := [\log(q_1/q_k), \dots, \log(q_{k-1}/q_k)] \in \mathbb{R}^{k-1}$  that maps from the simplex  $\Delta_k$  to the Euclidean space  $\mathbb{R}^{k-1}$  [42]. The inverse is the logistic transform

$$q = \left[ \frac{\exp(q'_1)}{z_k}, \dots, \frac{\exp(q'_{k-1})}{z_k}, \frac{1}{z_k} \right] \in \Delta_k \quad \text{where} \quad z_k = 1 + \sum_{j=1}^{k-1} \exp(q'_j).$$

The logistic normal distribution on the original parameter  $q$  corresponds to a normal distribution on the transformed parameter  $q'$  by change of variable [42]. By change of variable, the individual-level posterior on  $q'$  conditional on each individual observed response  $y_i$ , with the prior in Example 2, is

$$\mu_i(q') = p(q' | y_i) \propto \left( \frac{1}{z_k} \right)^{[y_i=k]} \times \prod_{j=1}^{k-1} \left( \frac{\exp(q'_j)}{z_k} \right)^{[y_i=j]} \times \exp \left( -\frac{1}{2} \frac{\|q'\|^2}{10^2} \right)$$

up to the normalising constant, where  $[y_i = j]$  is 1 if  $y_i$  is the  $j$ -th class label and 0 otherwise.

We provide a brief description of each algorithm used in comparison with WGBost. MCDropout and DEnsemble are described in Appendix E.2.

- DDistillation [57] predicts the parameter of a Dirichlet distribution over the simplex  $\Delta_k$  by a neural network using the output of DEnsemble. The output of multiple networks in DEnsemble is distilled into the a Dirichlet distribution controlled by one single network.
- PNetwork [14] considers the case where the individual-level posterior of the categorical response distribution falls into a Dirichlet distribution similarly to deep evidential learning [11]. It predicts the hyperparameter of the individual-level posterior given in the form of the Dirichlet distribution.

### E.4 Choice of Initial State of WGBost

In standard gradient boosting, the initial state at step  $m = 0$  is specified by a constant that most fits given data. Similarly, we specified the initial state  $\{\vartheta_0^n\}_{n=1}^N$  of WEvidential by a set of constants that most fits the output distributions in average. We find such a set of constants by performing an approximate Wasserstein gradient flow averaged over all the output distributions. Specifically, given the term  $\mathcal{G}_i(\mu)$  in Algorithm 1, we define  $\bar{\mathcal{G}}(\mu) := (1/D) \sum_{i=1}^D \mathcal{G}_i(\mu)$  and perform the update scheme of a set of  $N$  particles  $\{\bar{\vartheta}_m^n\}_{n=1}^N$ :

$$\begin{bmatrix} \bar{\vartheta}_{m+1}^1 \\ \vdots \\ \bar{\vartheta}_{m+1}^N \end{bmatrix} = \begin{bmatrix} \bar{\vartheta}_m^1 \\ \vdots \\ \bar{\vartheta}_m^N \end{bmatrix} + \nu_0 \begin{bmatrix} -[\bar{\mathcal{G}}(\hat{\pi}_m)](\bar{\vartheta}_m^1) \\ \vdots \\ -[\bar{\mathcal{G}}(\hat{\pi}_m)](\bar{\vartheta}_m^N) \end{bmatrix}$$

with the learning rate  $\nu_0 = 0.01$  up to the maximum step number  $m = 5000$ . The initial particle locations for this update scheme were sampled from a standard normal distribution. We specified the initial state  $\{\vartheta_0^n\}_{n=1}^N$  by the set of particles  $\{\bar{\vartheta}_m^n\}_{n=1}^N$  obtained though this scheme at  $m = 5000$ .